consider 41 jointly with the trimethoxychalcones in subsequent SAR analysis.

However, the PLS analysis of these compounds together with 11 physicochemical descriptors did not give a significant model (model 1, $r^2 = 0.497$, $q^2 = 0.000$). The t-u score plot, which displays the observations in the projected X(t) and Y(u) space and shows how well the Yspace (biological activity) correlates to the Xspace (descriptors), identified five possible outlier compounds (4, 11, 13, 28, 129). Omission of these compounds resulted in an improved model 2 that could account for 77% and predict 38% of the antimalarial activity of the series (Table 4 in Supporting Information). With 11 descriptors, it is likely that some descriptors would be less important. A measure of the relative importance of the X variables is calculated as VIP (variable importance in the projection), which is available in SIMCA. Each variable has a VIP value that is indicative of its relative importance in accounting for activity, with variables having VIP > 1 making a greater contribution. 13 The omission of variables based on the VIP values was done cautiously because it is possible to omit too many variables and to derive an apparently good model without sound predictive power. The VIP plot was viewed together with the coefficients and loading plots. Natural "thresholds" in the VIP plot was particularly useful in discriminating between important and unimportant parameters. In most cases, a VIP cutoff value of about 0.7 was applied. On the basis of these criteria, the variables branching, molar refractivity, difference in 13C chemical shift of carbonyl carbon, log A, and log V were not found to contribute significantly to model 2, and their removal might result in an improved and simplified model. Of the remaining descriptors, the hydrophobicity parameters (ClogP and log kw) have comparable VIP values (0.935, 0.911). It was decided that only one parameter would be retained in the final model, and $log k_w$ was arbitrarily chosen. Model 2 was thus reevaluated with a smaller number (five) of physicochemical parameters. An improvement was noted in the new model 3, which had better predictive ability (q^2 = 0.595, Table 4 in Supporting Information).

The predictive power of model 3 was further evaluated by selecting a few compounds from this model and using them as the "training set" to predict the activity of the remaining (unselected) compounds. The choice of the training set compounds was made by considering the score plot of model 3 (Figure 1 in Supporting Information). Six compounds were selected to form the training set (model 4, $r^2 = 0.985$, $q^2 = 0.723$), and it was able to predict the activity of the remaining eight compounds reasonably well, as seen from the root-mean-square error of prediction (RMSEP = 0.276). When used to predict the activity of all the trimethoxychalcones (n = 14, including five outliers but excluding the training set compounds), the error of prediction rose to 0.514.

A closer look at model 3 showed that electronic parameters are the main contributors to the antimalarial activity of the trimethoxychalcones. The five parameters, in order of increasing importance, were dipole moment $\leq \log k_w \leq$ charge on carbonyl oxygen \leq HOMO \leq LUMO, and they were inversely related to activity (Figure 2). Thus, one would expect good activity in a trimethoxychalcone that has low energies for its

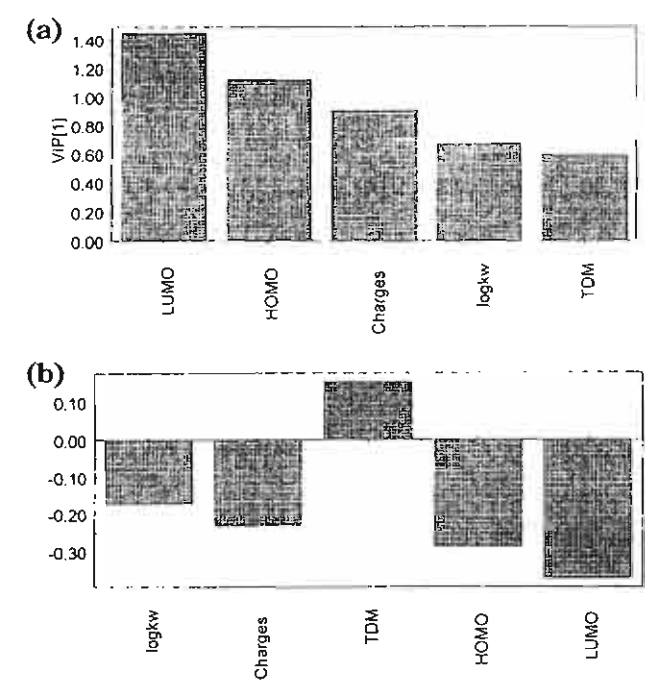


Figure 2. (a) VIP plot from PLS analysis of data from model 3 and (b) coefficients plot from PLS analysis of data from model 3. Parameters with positive coefficient values relate directly to activity, while those with negative coefficients are inversely related to activity. In this plot, only the dipole moment (TDM) is directly related to activity. LUMO = lowest empty molecular orbital; HOMO = highest occupied molecular orbital; charges = charge on carbonyl oxygen; $\log k_w = \text{hydrophobicity parameter}$ obtained from reversed-phase HPLC, where k_w is the capacity factor in 100% water; TDM = total dipole moment.

lowest empty and highest occupied molecular orbitals, a weakly polarized carbonyl function that would result in a small charge on the carbonyl oxygen, small total dipole moment, and low lipophilicity. The energies of HOMO and LUMO serve as indices of the electrondonating and electron-acceptor abilities of the molecule, respectively. The higher the energy of the HOMO is, the better its electron-donating ability. In the case of LUMO, good electron-acceptor ability is associated with low-energy molecular orbitals. In this case, activity is inversely related to both HOMO and LUMO, which suggests that electron-acceptor ability, rather than electron-donor ability, is important in determining activity. Electron-withdrawing substituents on ring A would make the ring electron-deficient and a better electron acceptor and, according to the present structureactivity relationship, would give rise to a more active antimalarial chalcone. The inductive and mesomeric effect of the electron-deficient ring could be transmitted along the $\alpha\beta$ unsaturated carbonyl chain, resulting in a less polarized carbonyl linkage. This would explain the inverse relationship between activity and the negative charge on the carbonyl oxygen (i.e., good activity is associated with a small negative charge on the carbonyl oxygen).

(b) Methoxychalcones. The most active compound in this series is 1-(4'-methoxyphenyl)-3-(3-quinolinyl)-2-propen-1-one (31), with an IC₅₀ of 4.8 μ M. The association of the 3-quinolinyl ring with good activity is an interesting recurring feature among all four series of alkoxylated chalcones. The methoxychalcone with an

unsubstituted A ring (135) has poor antimalarial activity (IC₅₀ = 55.5 μ M). Substitution of the A ring with polar, electron-withdrawing groups such as nitro (115) and cyano (117) results in a further reduction of activity. Substitution with other groups resulted in either improvement or little change in activity, and this aspect was investigated in greater detail with PLS.

A significant PLS model 5 was obtained only after omission of some "outlier" compounds from the series. These outliers were detected visually from the PLS score (t-u) of all 14 methoxychalcones as well as from the residual values of the model. In this way, 19, 31, 113 were identified as outliers. There is some concern over the omission of 19 and 31 because these compounds are among the three most active compounds (IC₅₀ < 10μ M) in the series. However, their omission was necessary to give a significant one-component model 5, which accounted for 63% and predicted 32% of antimalarial activity. As before, the model was improved by omitting less important descriptors identified from the VIP and coefficients plot. The improved model 6 could predict the activity of 11 methoxychalcones using 5 descriptors with a q^2 of 0.585. The predictive power of the model was further confirmed by selecting a training set of five compounds (model 7), and using it to predict activity of the remaining six compounds (RMSEP = 0.283). The training set was also used to predict the activity of all the methoxychalcones (n = 9, including three outliers). Prediction was only satisfactory with an RMSEP of 0.520

The VIP plot of model 6 identified branching, $\log k_{\rm w}$, and HOMO as the parameters (in order of decreasing importance) contributing to the activity of the methoxychalcones. Activity was directly related to branching (i.e., disubstitution of A ring) and HOMO, but inversely related to $\log k_{\rm w}$. The emphasis on the branching parameter may be biased because there are only two compounds (111, 113) with disubstituted A rings in model 5. Moreover, with the omission of 19 and 31 (both active and monosubstituted A ring compounds) as outliers, 113 is the only remaining "active" compound (IC50 < 10 μ M) in model 6, and this may have led to undue emphasis on the state of substitution of ring A.

The lipophilicity parameter $\log k_{\rm w}$ is important in determining activity. As in the case of the trimethoxychalcones, the relationship is inverse; i.e., lower lipophilicity in the compound favors good antimalarial activity. The direct correlation between activity and HOMO suggests that the electron-donating ability of the chalcone is important for good activity. An interesting observation is the relationship that exists between HOMO and $\log k_{\rm w}$ (r = -0.590, p < 0.05). This would suggest that the electronic parameter may be the single most significant parameter influencing activity.

(c) Dimethoxychalcones and Ethoxychalcones. The initial PCA score plot of the alkoxylated chalcones (Figure 1a) indicated an overlapping distribution of the dimethoxy- and ethoxychalcones. Therefore, there was good reason for considering these two series together in subsequent analyses. However, no significant PLS model could be obtained, and it was decided that they should be evaluated separately.

The ethoxychalcones are outstanding in that no active compound (IC₅₀ < 10 μ M) has been identified from this

series. The unsubstituted A ring ethoxychalcone (136) has poor activity (IC $_{50} = 43 \,\mu\text{M}$), and activity is further depressed by substitution or replacement with 4-cyano (127), 2,4-dichloro (121), and 4-quinolinyl (34). The most active compounds were the 3-quinolinyl (33) and 4-trifluoromethyl (122) derivatives, the same A ring substituents that were earlier identified as "actives" for the trimethoxy and methoxy (only for 3-quinolinyl) series. No significant PLS model could be obtained even after removing outliers or reducing the number of descriptors. This means that the present descriptors cannot adequately describe the variation in activity of the ethoxychalcones and that new variables should be found to define activity.

The dimethoxy series is outstanding in having the greatest representation of active alkoxylated chalcones (5 out of 12) in this investigation. A significant PLS model 8 was derived after omitting five outlier compounds (5, 103, 106, 104, 110) ($r^2 = 0.694$, $q^2 = 0.486$). and this was further improved when descriptors that contributed little to activity (identified through coefficient and VIP plots) were omitted from the model. The final model 9 accounted for 68% and predicted 61% of activity. As before, a training set (model 10) was selected from these 12 compounds and was used to predict the activity of the remaining 7 compounds. Only a satisfactory prediction was obtained in this case (RMSEP = 0.689). Prediction was poorer (RMSEP = 1.346) when the training set was applied to the entire cohort of dimethoxychalcones (n = 12, including outliers). The main parameters influencing the activity of dimethoxychalcones were the size parameters (log A, log V), which have VIP values greater than 1. The other parameters, in order of decreasing importance, were $\log k_w$, molar refractivity, and HOMO. Except for $log k_w$, the other parameters affected activity directly.

(d) Hydroxychalcones and Dihydroxychalcones. The 30 hydroxylated chalcones were found to be homogeneous in terms of the principal components summarizing their independent descriptors. This is seen from their PCA score plot (Figure 1b), which showed a smooth integration of compounds of both series within the confines of the four quadrants. Nevertheless, attempts were also made to analyze the two series separately. Both approaches had several similarities. For example, the VIP plots identified dipole moment and a lipophilicity parameter as being important for the activity of each series, whether considered separately or together. However, the small size of the dihydroxy series (n = 11) posed difficulties in developing a training set. Therefore, it was decided that the two series should be considered together.

Applying PLS to the hydroxy and dihydroxychal-cones proved to be difficult without eliminating a large number of compounds as outliers. To avoid this, a training set of compounds was directly selected from the 30 hydroxylated chalcones (model 11). The number of descriptors in this model was then reduced, and the final training set comprised 17 compounds and 4 descriptors (dipole moment, branching, molar refractivity, $\log k_w$) (model 12: $r^2 = 0.818$, $q^2 = 0.602$). It was able to predict the activity of the remaining 13 compounds with a satisfactory level of accuracy (RMSEP = 0.425).

The coefficient, loadings, and VIP plots of model 12 identified four descriptors as being important determinants of activity. These were dipole moment, branching, molar refractivity, and log kw, in order of decreasing importance. Of these four descriptors, dipole moment and log kw influenced activity directly while branching (disubstitution of ring A) and molar refractivity affected activity inversely. Because molar refractivity is significantly correlated (p < 0.01) to size parameters for this series, the requirements for good activity in hydroxylated chalcones would be the presence of polar and small-sized substituents, which were different from that observed in the 4'-methoxy and 2',4'-dimethoxy series.

(e) Active Hydroxylated and Alkoxylated Chalcones. In a final analysis, the active members of the hydroxylated and alkoxylated chalcones (a total of 19 compounds) were gathered to form a separate series. This was prompted by observations from the PLS score plots of the five series prior to weeding out outliers and trimming the number of descriptors. It was noted that some of the active compounds tended to be outliers. In the methoxy series, two out of the three compounds removed as outliers were active compounds (IC₅₀ < 10 μ M). In the dimethoxy series, one active compound was removed because of its outlying position. In addition, when the predictive ability of the training sets of each series was evaluated, it was noted that many of the active compounds had large residual values; i.e., their activities were poorly predicted by the proposed model. Therefore, an analysis of all the active compounds as a series would be useful in revealing if they share common characteristics. A PLS analysis of the 19 active compounds using 10 descriptors (13C chemical shift of the carbonyl carbon was omitted because only four compounds have this descriptor) gave a significant onecomponent model 13 ($r^2 = 0.677$, $q^2 = 0.563$). This model was further improved by removing descriptors that had VIP values of less than 0.25 (viz. HOMO, LUMO, and branching) to give model 14, which had improved predictive power ($q^2 = 0.598$). A training set of eight compounds was selected from the score plot of model 14, which is depicted in Figure 2a (Supporting Information). The training set (model 15, $r^2 = 9.957$, $q^2 = 0.833$) was able to predict the activity of the remaining active compounds with an RMSEP value of 0.299 (Figure 2b in Supporting Information). The main descriptors important for activity (in order of importance) were the size parameters (log A, log V, molar refractivity; these parameters are significantly correlated to each other, p < 0.01) and log k_w . Therefore, size and lipophilicity are important features of the active chalcones. However, stepwise multilinear regression only identified size (log A) as an important parameter for describing in vitro activity of these active chalcones:

$$-\log IC_{50} = (6.35 \pm 1.07)\log A - (10.57 \pm 2.64)$$

 $n = 19$, $r^2 = 0.690$, $r_{cv}^2 = 0.616$, SE = 0.202,
SE_{cv} = 0.225, $F = 35.567$

The emphasis on size for good activity must be considered in light of both rings A and B. Among the active chalcones, there is a strong representation from the trimethoxy and dimethoxy series, which have bigger size B rings. This is in compliance with the regression equation. However, bigger size A rings do not always result in more active compounds. For example, although the quinoline ring is comparable in size to the naphthalene ring, there are no active naphthalene A ring derivatives but several active quinolinyl A ring derivatives. Furthermore, only 3-quinolinyl, and not 4-quinolinyl derivatives, are active chalcones. This makes the good activity of the 3-quinolinyl A ring derivatives and chalcones with comparatively small size A rings (e.g., 4-fluorophenyl 36, 4-trifluoromethylphenyl 2, 6, 4-hydroxy 19) quite exceptional. It may be related to the hydrophobicity parameter $\log k_w$, which was identified as an important parameter from the PLS model 15. On the basis of the correlation matrix drawn up for the descriptors of the active compounds, $\log k_w$ is not correlated to any of the size parameters. It may reflect the polarity of the compound because the determination of log kw depends on its elution from a hydrophobic column with a polar mobile phase.

Discussion

Six series of chalcones, broadly classified according to the substitution pattern of the B ring, have been investigated for in vitro antimalarial activity. Within each series, the other aromatic ring (ring A) is substituted with a wide range of groups of varying lipophilicities and electronic character or is replaced by heteroaromatic or bicyclic ring systems. The physicochemical properties and in vitro activities of these compounds cover a considerable range, a feature that would ensure that a comprehensive and meaningful structure-activity relationship could be carried out.

"Nineteen compounds have been identified as "actives" from the present study. These comprise 12 alkoxylated chalcones (IC₅₀ < 10μ M) and 7 hydroxylated chalcones (IC₅₀ < 20 μ M). The latter series have weaker antimalarial activity when compared to their alkoxylated analogues, and a lower criteria for activity is defined for these compounds. The most active compound to emerge from this study is 1-(2',3',4'-trimethoxyphenyl)-3-(3-quinolinyl)-2-propen-1-one (27), with an IC_{50} of 2 μ M. An interesting observation is the association of good antimalarial activity with the 3-quinolinyl A ring derivatives. This is observed across several ring B series but not with the 4'-hydroxylchalcones. The quinoline ring is a common entity in established antimalarials. It may play a role in facilitating the localization of the drug within the acidic food vacuole of the parasite because of its basic properties. The planar and aromatic quinoline ring would enhance π - π stacking to the porphyrin rings in heme, which is widely held to be a potential target for quinoline-containing antimalarial agents.15 The quinoline A ring in the chalcones may have similar roles. A steric element is possibly involved in the interaction because 4-quinolinyl A ring derivatives are significantly less active than their 3-quinolinyl counterparts. It would be of interest to investigate the heme-binding properties of these chalcones to assess the contribution of the quinoline ring to the overall process.

The antimalarial activity of the active chalcones was evaluated in P. berghei infected mice. Several of the chalcones increased the survivability of the mice relative to control infected mice treated with either DMSO or 41, but only a few were comparable to chloroquine in

this respect. Among the active chalcones, the in vivo activity of **8** (2',4'-dimethoxy-4-ethylchalcone) is noteworthy. More surprising is the good in vivo activity of **208**, 1-(2',4'-dihydroxy)-3-(4-naphthalenyl)-2-propen-1-one, which was not identified as an active chalcone in view of its high IC₅₀ (20 μ M). Poor in vitro and in vivo correlation is a problem in the evaluation of antimalarial potency and may be attributed to the pharmacokinetics of the test compound and differences in the strain of plasmodia used for the tests.

Previous structure—activity studies on the antimalarial activity of chalcones have reported a preference for electron-acceptor groups (such as dichloro or difluoro at the 2,3 or 2,4 positions) in the A ring for good activity.⁵ Our present study suggests that this is not necessarily so. The substitution of the B ring is important in determining the type of A ring substituents that would give optimum antimalarial activity. For example, 2,4-dichloro substitution of ring A in the trimethoxy-chalcones gave rise to a very active compound (3, IC $_{50}$ = 5.4 uM), but the same substituent gave rise to less active compounds in other series of chalcones (1, 111, 121, 201, 229).

The structure-activity analysis has been carried out using the multivariate data analytical tools PCA and PLS. The distribution of the alkoxylated chalcones in the PCA score plot suggests that each series should be considered separately. Fairly predictive PLS models have been developed for each class of alkoxylated chalcone, with the exception of the ethoxychalcones. The structural requirements of each series are different, confirming our initial observation that the nature of the B ring is critical in determining the overall structural requirements for activity. Thus, size parameters were important for the dimethoxychalcones while electronic characteristics (electron-withdrawing groups) were more important considerations for the methoxy- and trimethoxychalcones. The hydroxy- and dihydroxychalcones were considered together as a class, and in this case, small size and polarity were important considerations for good activity. The PLS models developed for each class have several limitations. For example, satisfactory models could be obtained only upon omission of outlier compounds. This may be due to the inadequate coverage afforded by the descriptors used in the present analysis, as well as the small size of compounds representing each class.

A separate analysis was also carried out on the 19 active compounds because many of them appeared to be outliers in their respective series. Surprisingly, a better PLS model was obtained for the active compounds than for the individual B ring series. This model 14 was able to account for 67% and predict 60% of the activity. A training set (model 15) selected from this model predicted the activity of the remaining compounds with an error (RMSEP) of 0.299. Size and hydrophobicity (log kw) factors were important parameters for activity. The results suggest that size considerations are dominated by the B ring while the A ring may be more important in influencing hydrophobicity, which in this instance may reflect the polar characteristics of the molecule. Moreover, the association of 3-quinolinyl ring A chalcones with good antimalarial activity would make

the ring A/B heterocyclic chalcones particularly attractive candidates for antimalarial activity.

In conclusion, MVA tools have been used in the present study to delineate the structural requirements for antimalarial activity in oxygenated and alkoxylated chalcones. PLS models with reasonably good predictive values have been developed for each series, and the results may be applied to designing drugs with improved antimalarial activity.

Experimental Section

Chemistry. Melting points were uncorrected. Elemental analyses and accurate mass determinations were carried out by the Department of Chemistry, National University of Singapore. Elemental analyses are indicated by symbols (C, H, N) if they are within $\pm 0.4\%$ of the theoretical values. Mass spectra were collected on a VG Micromass 7035 E mass spectrometer by chemical ionization methods. IR spectra (pressed KBr disks or neat) were recorded on a JASCO FTIR-430 instrument. Chemical shifts of ^1H NMR spectra, which were obtained on a Bruker (DPX 300 MHz) spectrometer, are reported in δ (ppm) relative to tetramethylsilane as the internal standard. Thin-layer chromatography of the final compounds were done on silica gel sheets (with fluorescent indicator) using CHCl3 or CHCl3/hexane (4:1 or 3:2) as eluting solvents.

Chemical Syntheses. (a) Alkoxylated Chalcones. The general procedure for preparing the alkoxylated chalcones is as follows. In a round-bottom flask, a methanolic solution of NaOH (3% w/v, 10 mL) and the substituted aldehyde (10 mmol in 10 mL) were stirred together at room temperature (28 °C). A methanolic solution of the substituted acetophenone (10 mmol, 10 mL) was added dropwise, and the mixture was stirred for 12-18 h. The alternative method of adding the aldehyde to a stirred solution of the acetophenone in alkaline methanol did not result in any significant difference in yield. In most cases, the product was obtained as a brightly colored precipitate after a short period of stirring. The precipitate was removed by filtration, washed with cold methanol, and recrystallized. When no precipitate was obtained, the solution was diluted with water, neutralized with HCl, and extracted with ethyl acetate. The organic layer was dried with anhydrous Naz-SO4 and removed by evaporation under reduced pressure to give either a solid or liquid residue. The solid residue is treated as above. The liquid residue is passed through a column of silica gel (230-400 mesh ASTM) and eluted with CHCl₃ or CHCl3/hexane. For all compounds, recrystallization was done twice and purity was checked by TLC before characterization by 1H NMR, IR, and accurate mass and elemental analyses. The yields of the synthesized compounds, their melting points, and spectroscopic and elemental analyses data are given in the Supporting Information (Table 1).

(b) Hydroxylated Chalcones. A solution of 4-hydroxyacetophenone or 2,4-dihydroxyacetophenone (10 mmol), pyridinium *p*-toluenesulfonate (0.4 mmol), and 2*H*-3,4-dihydropyran (16 mmol) in methylene chloride (20 mL) was stirred for 4 h at room temperature. A solution of Na₂CO₃ (1 M, 20 mL × 2) was then added to wash the reaction mixture. The organic layer was separated, combined together, dried over anhydrous Na2SO4, and concentrated in vacuo to give the crude tetrahydropyranyl ether as a yellow to white product (solid or liquid). The crude tetrahydropyranyl ether was characterized by 'H NMR to confirm its formation and was used without further purification for reaction with the appropriate aldehyde. A methanolic solution of the ketone protected as tetrahydropyranyl ether (10 mmol, 10 mL) was added to a stirred solution of the aldehyde (10 mmol) in methanol (5 mL) at room temperature. This was followed by dropwise addition of a methanolic solution of sodium hydroxide (3% w/v, 10 mL). Stirring was continued for 12-18 h, and the reaction mixture was worked up as described earlier for alkoxylated chalcones, to give the crude protected hydroxylchalcone. Acid (4 M HCl, 4 mL) was added to a stirred solution of the crude product (2

0.2 mmol) in absolute alcohol (10 mL), and the mixture was stirred for 4 h at room temperature and then diluted with water (40 mL). The mixture was extracted with ethyl acetate (50 mL × 3), and the combined organic phases were concentrated in vacuo to give the crude hydroxylated chalcone. The crude product was purified by column chromatography using silica gel (230-400 mesh ASTM) as the stationary phase and CHCl/hexane as the mobile phase. For all compounds, recrystallization was done twice and purity was checked by TLC before characterization by 1H NMR and accurate mass and elemental analyses. The yields of the synthesized compounds, their melting points, and spectroscopic and elemental analyses data are given in the Supporting Information (Table 1)

Evaluation of in Vitro Antimalarial Activity. The in vitro antimalarial activities of compounds 1-92 were evaluated by the method of Desjardins et al.,16 with modifications. Briefly the assay measures the incorporation of [3H] hypoxanthine by the parasites and the inhibition of the incorporation in the presence of the test compound. A strain of chloroquine resistant (K1) Plasmodium falciparum was used in the assay. The test compounds were dissolved in DMSO and serially diluted 10-fold with complete culture media (RPMI-1640, 5% sodium bicarbonate, and 10% normal type "O" human serum) to give a 106-fold concentration range. The diluted drugs (25 μL) were transferred to wells in a 96-well microtiter plate, together with 200 µL of parasitized erythrocytes (1-2% parasitemia and 1.5% hematocrit), and the whole was incubated at 37 °C for 24 h in a candle jar. The control well in each plate contained 25 µL of complete medium instead of the test compound. Chloroquine was also tested as a positive control. After 24 h, 25 μ L of [3 H] hypoxanthine was added, and the plates were incubated for an additional 24 h, after which the cells were filtered onto glass fiber filters (Whatman 934-AH) and counted in a scintillation counter. For each test compound, the concentration-response profile was determined and analyzed by a nonlinear, logistic dose response program to give its IC50, which is the concentration of test compound required to inhibit [3H] hypoxanthine uptake by 50% compared

Evaluation of in Vivo Antimalarial Activity. The in vivo test measures the survivability of mice following administration of the drug. Swiss albino mice (male, 4 weeks, approximately 25 g) were inoculated intraperitoneally with 107 parasitized erythrocytes (P. berghei ANKA). The test compound was given intraperitoneally at a daily dose of 100 mg/ kg in DMSO for 3 consecutive days after the day of infection (day 0). Each compound was tested against three mice. Three groups of control infected mice were maintained, and they were given chloroquine (52 mg/kg, ip, 0.5% Tween buffer solution, pH 7.4) on day 1 and DMSO or 41 (2,4-dimethoxy-4'-butoxychalcone, 100 mg/kg in DMSO, ip) on days 1-3. Thin blood smears were made from the tail blood of the mice from day 1 to day 14 or until their demise. The blood smears were fixed with 5% Giemsa, examined microscopically, and graded according to WHO protocol for evaluating the degree of parasitemia.17 Control infected mice treated with DMSO or chloroquine would normally perish within 8 days and 14-16 days, respectively. Mice that received 41 would live on the average for 8-9 days.

Determination of Lipophilicity by Reversed-Phase HPLC. Lipophilicity was determined experimentally from their capacity factors (K) by a reversed-phase HPLC method. Separation was achieved on a LiChrosorb RP-18 (10 µM) stationary phase with a methanol/0.02 M phosphate buffer (pH 7.0) mobile phase. At least four mobile-phase compositions were investigated for each compound, with the methanol content ranging from 50% to 85% w/w for each composition. Determinations were carried out at 30 °C, with the flow rate adjusted to 1.0-1.5 mL/min depending on the mobile-phase composition, with UV detection set at 280 and 330 nm. A stock solution (10 mg/mL) of the compound was prepared in methanol. For each mobile phase composition, equal volumes (20 μ L) of the stock solution and an acetone stock solution (10% v/v acetone in the mobile phase) were diluted to 200 µL with the

mobile phase and an aliquot (10 μ L) was injected for the determination of retention time. Triplicate determinations were done for each concentration of test compound at each mobile-phase composition. The capacity factor (K) was determined from $\log K = \log[(V_s - V_o)/V_o]$, where V_s and V_o are the retention volumes of the test compound and acetone, respectively. Linear regression of $\log K$ of each compound against mobile-phase composition and extrapolation to 100% aqueous phase gave $\log k_w$ of the compound at pH 7.0.

Determination of the Chemical Shift of the Carbonyl Carbon. 13C NMR spectroscopy was used to determine the chemical shift of the carbonyl carbon in the trimethoxy series of chalcones. The difference in chemical shift is given by $\Delta \delta =$ $\delta_X - \delta_R$, where δ_X is the chemical shift of the trimethoxychalcone with a substituted A ring and δ_R is that of the reference compound (2',3',4'-trimethoxychalcone with no A ring substitution, 189.976 ppm). $\Delta\delta$ is known to be sensitive to the electronic influence of the alkyl/aryl moieties 18,19 and is used here to give a direct assessment of the electronic effects of the A ring, which is attached by conjugation to the carbonyl carbon. The 13C NMR spectra of the chalcones (CDCl3 or dimethyl-ds sulfoxide, tetramethylsilane as reference) were determined on a Bruker ACF 300 instrument.

Molecular Modeling Methods. The following parameters were determined from the force-field-minimized geometries of the chalcones using the SYBYL 6.6 force field MMFF94 (Tripos Associates, St Louis, MO), with calculations continued until the rms gradient was less than 0.001 kcal mol-1 A: ClogP. molecular refractivity (MR), total dipole moment (TDM), Connolly surfaces (volume and surface area, calculated from MOLCAD in SYBYL), and negative charge on the carbonyl oxygen using the Gasteiger-Huckel method. Orbital energies for HOMO and LUMO were calculated from MOPAC (OCPE program 455, version 6.0), which is interfaced with SYBYL.

Statistical Methods. Multiple linear regression analyses were carried out using SPSS 10 (SPSS, Inc., Chicago, IL). The following statistical parameters were determined for each regression equation: 95% confidence interval variables, measure of explained variance r^2 , Fischer significance ratio F at P = 0.05, and standard error SE. Cross-validated r^2 and SE were determined using the QSAR module of SYBYL 6.6.

Multivariate data analyses were performed with SIMCA-P (version 8.0)20 using default settings.

Acknowledgment. Mei Liu gratefully acknowledges the National University of Singapore for granting her a research scholarship. This work has been supported by Grant RP-140-000-016-112 from the National University of Singapore (M.-L.G.) and the Thailand Research Fund (P.W.).

Supporting Information Available: Tables containing physical and analytical data of synthesized compounds (Table 1), their physicochemical descriptors (Table 2), correlation maxtrix of descriptors (Table 3) and a summary of PLS models (Table 4) and figures showing the score plots of principal components for alkoxylated chalcones (Figure 1), PLS score plots for actives (Figure 2a), and a plot of predicted vs observed activities of actives (Figure 2b). This material is available free of charge via the Internet at http://pubs.acs.org.

References

(1) Wahlgren, M.; Bejarano, M. T. A blueprint of "bad"air". Nature 1999, 400, 506-507.

Malaria Foundation International, Roll Back Malaria. http:// www.malaria.org/RBM.html.

Chen, M.; Theander, T. G.; Christensen, B. S.; Hviid, L.; Zhai, .; Kharazmi, A. Licochalcone A, a new antimalarial agent inhibits in vitro growth of the human malaria parasite Plasmo-dium falciparum and protects mice from P. yoelii infection.

dium falciparum and protects mice from P. yoelii infection. Antimicrob. Agents Chemother. 1994, 38, 1470–1475. Chen, M.; Christensen, S. B.; Zhai, L.; Rasmussen, M. H.; Theander, T. G.; Frokjaer, S.; Steffansen, S.; Davidsen, J.; Kharazmi, A. The novel oxygenated chalcone, 2,4-dimethoxy-4'-butoxychalcone, exhibits potent activity against human malaria parasite *Plasmodium yoelii in vivo. J. Infect. Dis.* **1997**, *176*, 1327–1333.

- (5) Li, R.; Kenyon, G. L.; Cohen, F. E.; Chen, X.; Gong, B.; Dominguez, J. N.; Davidson, E.; Kurzban, G.; Miller, R. E.; Nuzum, E. O.; Rosenthal, P. J.; McKerrow, J. H. In vitro antimalarial activity of chalcones and their derivatives. J Med. Chem. 1995, 38, 5031-5037.
- Ram, V. J.; Saxena, A. S.; Srivastava, S.; Chandra, S. Oxygenated chalcones and bischalcones as potential antimalarial agents. Bioorg. Med. Chem. Lett. 2000, 10, 2159–2161.
- Nielsen, S. F.; Christensen, S. B.; Cruciani, G.; Kharazmi, A.;
- Liljefors, T. Antileishmanial chalcones: statistical design, synthesis and three-dimensional quantitative structure—activity relationship analysis. *J. Med. Chem.* 1998, 41, 4819—4832. Herencia, F.: Ferrandiz, M. L.; Ubeda, A.; Dominguez, J. N.; Charris, J. E.; Lobo, G. M.; Alcaraz, M. J. Synthesis and anti-inflammatory activity of chalcone derivatives. *Bioorg. Med. Chem.* 1998, 2, 1160, 1124.
- Chem. Lett. 1998, 8, 1169-1174.

 Ducki, S.; Forrest, R.; Hadfield, J. A.; Kendall, A.; Lawrence, N. J.; McGown, A. T.; Rennison, D. Potent antimitotic and cell growth inhibitory properties of substituted chalcones. *Bioorg. Med. Chem. Lett.* 1998, *8*, 1051–1056.

 [10] Bois, F.; Boumendjel, A.; Mariotte, A.; Consell, G.; Di Petro, A.
- Synthesis and biological activity of 4-alkoxychalcones: potential hydrophobic modulators of P-glycoprotein-mediated multidrug resistance. *Bioorg. Med. Chem.* 1999, 7, 2691–2695. (11) Hsieh, H. K.; Lee, T. H.; Wang, J. P.; Wang, J. J.; Lin, C. N.
- Synthesis and anti-inflammatory effect of chalcones and related compounds. *Pharm. Res.* 1998, 15, 39-46.
- van de Waterbeemd, H. Quantitative approaches to structure—activity relationships. In *The Practice of Medicinal Chemistry*, Wermuth, C. G., Eds.; Academic Press: London, 1996; pp 367—

- (13) Wold, S.; Johansson, E.; Cocchi, M. PLS-Partial least-squares projections to latent structures. In 3D QSAR in Drug Design: Theory. Methods and Applications, Kubinyi, H., Ed.; Kluwer/ Escom: Dordrecht, The Netherlands, 2000; pp 523-550.
- (14) Winiwarter, S.; Bonham, N. M.; Ax, F.; Halberg, A.; Lennernas, H.; Karlen, A. Correlation of human jejunum permeability (in vivo) of drugs with experimentally and theoretically derived parameters. A multivariate data analysis approach. J. Med. Chem. 1998. 41, 4939-4949.
- (15) O'Neill, P. M.; Bray, P. G.; Hawley, S. R.; Ward, S. A.; Park, B. K. 4-Aminoquinolines-Past, Present and Future: A Chemical
- Perspective. Pharmacol. Ther. 1998, 77, 29-58.
 (16) Desjardins, R. E.; Canfield, C. J.; Haynes, D. E.; Chulay, J. D. Quantitative assessment of antimalarial activity in vitro by a semiautomated microdilution technique. Antimicrob. Agents Chemother. 1979, 16, 710-718.
- (17) World Health Organisation. Basic Malaria Microscopy. Part 1: A Learner's Guide, WHO: Geneva, 1991.
- (18) Wernly Chung, G. N.; Mayer, J. M.; Tsantili-Kakoulidou, A.; Testa, B. Structure-reactivity relationships in the chemical hydrolysis of prodrug esters of nicotinic acid. Int. J. Pharm. 1990, 63, 129-134.
- (19) Rong, X.; Go, M.-L. Structure-hydrolyzability relationships in a series of piperidinyl and tropinyl esters with antimuscarinic activity. Chem. Pharm. Bull. 1997, 45, 476-481.
- (20) SIMCA, Umetrics AB, Box 7960, S-907 19, Umea, Sweden, 1999. JM0101747

Molecular Defect of *PKD1* Gene Resulting in Abnormal RNA Processing in a Thai Family

NANYAWAN RUNGROJ, M.Sc.*, KRIENGSAK VAREESANGTHIP, M.D., Ph.D.**, PRAPON WILAIRAT, Ph.D.****, WANNA THONGNOPPAKHUN, Ph.D.*, CHINTANA SIRINAVIN, M.D.*,***, PA-THAI YENCHITSOMANUS, Ph.D.*,*****

Abstract

Autosomal dominant polycystic kidney disease (ADPKD) is a common human autosomal disorder caused mainly by mutations of the *PKD1* gene. In analysis of *PKD1* transcripts by long RT-PCR and nested PCR procedures, we observed *PKD1*-cDNA fragments from three ADPKD siblings from the same family with a size approximately 250 base pairs (bp) shorter than normal. Further investigations showed that the *PKD1* transcripts from these patients had been abnormally processed, the nucleotide sequence of exon 43 containing 291 nt was missing from the transcripts, which would result in an abnormal polycystin-1 with an in-frame deletion of 97 amino acids. This splicing defect did not result from a mutation that disrupted the splice donor or acceptor sites adjacent to exon 43 or the branch sites in flanking introns but was most likely due to 20-bp deletion observed in intron 43. The intronic deletion was present in 8 affected members but absent in 11 unaffected members, corresponding with the results of genetic linkage analysis using 5 polymorphic markers in the *PKD1* region. Molecular diagnosis of *PKD1* in this family could, therefore, be carried out by genomic DNA amplification to directly detect the *PKD1* intronic deletion.

Key word: Polycystic Kidney Disease 1 (*PKD1*), *PKD1* Mutation, Intronic Deletion, Exon Skipping, RNA Processing Defect, Abnormal Splicing

RUNGROJ N, THONGNOPPAKHUN W, VAREESANGTHIP K, SIRINAVIN C, WILAIRAT P, YENCHITSOMANUS P J Med Assoc Thai 2001; 84: 1308-1316

^{*} Division of Molecular Genetics, Department of Research and Development, Faculty of Medicine Siriraj Hospital,

^{**} Division of Nephrology, Department of Medicine, Faculty of Medicine Siriraj Hospital,

^{***} Division of Medical Genetics, Department of Medicine, Faculty of Medicine Siriraj Hospital,

^{****} Department of Biochemistry, Faculty of Science,

^{*****} Division of Medical Molecular Biology, Department of Research and Development, Faculty of Medicine Siriraj Hospital, Mahidol University, Bangkok 10700, Thailand.

Autosomal dominant polycystic kidney disease (ADPKD) is one of the most common human autosomal disorders, affecting approximately 1 per 1000 individuals. It is characterized by formation of multiple abnormal fluid-filled cysts in both kidneys, partly leading to end stage renal failure(1). ADPKD is genetically heterogeneous with at least three different genes (PKD1, PKD2, and PKD3) responsible for similar phenotypes(2-4). Abnormality of PKD1, which is located on chromosome 16p13.3, is the most common cause of ADPKD, accounting for approximately 85-90 per cent of cases(5), and appears to have a more severe effect with an early age of onset and end stage renal failure(6). Recent studies have shown that PKD1 probably occurs from two mutational events, germline and somatic mutations(7,8).

PKD1 has been isolated and characterized (9-12). Its size is 54 kb consisting of 46 exons and its mRNA transcript is composed of 14,148 nucleotides (nt). The predicted protein product, polycystin-1, contains 4,302 amino acids and is proposed to play a role in cell-cell or cell-matrix interaction(11). Approximately three-fourths of the sequence in the 5' region of PKD1 is reiterated with about 95 per cent similarity to three highly homologous genes mapped on 16p13.1, whereas, about one-fourth of the sequence in the 3' region is unique(9). This has complicated the characterization of PKD1 mutations. Although it is believed that most of the mutations occur in the reiterated region, the majority of mutations identified to date are located within the 3' unique region(9,13-15) and some 82 mutations have been characterized(16). The rate of mutation characterization has been slow and the number of mutation is too few for analysis of the correlation between type of mutation and variability of the PKD1 phenotype.

Recently, a long reverse transcription-polymerase chain reaction (RT-PCR) method has been developed for amplification and isolation of the entire *PKD1* coding sequence from peripheral blood lymphocytes⁽¹⁷⁾. This method is useful not only for the characterization of mutations occurring especially in the reiterated region of *PKD1* but also for the analysis of *PKD1* RNA processing and transcripts, without acquisition of kidney tissue. In this report, we describe a deletion mutation in intron 43 of *PKD1* which resulted in abnormal RNA processing involving exon 43 skipping in the *PKD1*

transcripts and also reported the development of a method for direct detection of this mutation in affected family members.

MATERIAL AND METHOD ADPKD Family and Linkage Analysis

The family described in this study (PK009) was one of approximately 50 Thai ADPKD families that have been identified and followed-up in the Department of Medicine, Faculty of Medicine Siriraj Hospital, Mahidol University. ADPKD was diagnosed according to established clinical and genetic criteria, based on the finding by ultrasonic scanning of polycystic kidneys with at least one cyst in one kidney and two or more in the other⁽¹⁸⁾, and the expression of the disease in members in consecutive generations of the family.

Blood samples (10-15 ml) were taken from ADPKD patients and family members with informed consent. Genomic DNAs were isolated from blood samples by standard method⁽¹⁹⁾ for linkage analysis and PCR amplification. Linkage analysis and haplotype characterization were performed by examinations of five polymorphic markers linked to *PKD1* on chromosome 16p, namely, D16S85 (3' HVR), KG8, SM6, 16AC2.5, and SM7(2,20-23).

RNA Isolation, cDNA Synthesis, and PCR

The methods for RNA isolation, full-length cDNA synthesis, long PCR, and nested PCR have previously been described⁽¹⁷⁾. Briefly, RNA was isolated from the lymphocytes by TRIzol[®] reagent (Life Technologies), and used for full-length cDNA synthesis with oligo (dT)₁₂₋₁₈ primer and RNase H-free reverse transcriptase. PKDI-cDNA was amplified by long PCR using a pair of primers (TH1F/TH1B; Table 1) and ELONGASETM Enzyme Mix (Life Technologies) containing thermostable Taq and Pfu polymerases. The length of PCR product was 13,634 bp (Fig. 1A).

Nested PCRs were performed by using 9 pairs of nested primers to generate 9 overlapping fragments. Sequences of nested PCR primers (SI9F/SI9B and WT5F/WT5B) used in this study are shown in Table 1. The others are available on request. The nested PCR products were analyzed by electrophoresis on 2 per cent LE agarose gel (FMC Corporation) in Tris-borate-EDTA (TBE) buffer. DNA fragments were stained with ethidium bromide, visualized on UV transilluminator, and photographed.

Table 1. Sequences of PCR primers for amplifications of PKDI.

Primer	Primer sequence (5'->3')	Nucleotide position	Location	PCR product size (bp)
Primers fo	or long RT-PCR			
THIF THIB	CTGGGGACGGCGGGCCATGCG GGCCTGGGGCAAGGGAGGATGACAA	175-196a 13808-13784a	5' UTR 3' UTR	13,634
Primers f	or nested PCR			
SI9F	CTTCAGCACCAGCGATTACGACGTT	11533-11557a	Exon 40	1,650
SI9B	AGAAAGTAATACTGAGCGGTGTCCACTC	13182-13155a	Exon 46	
WT5F	TTGGCTGGGAGAGTCCTCACAATG	11556-115792	Exon 40	817
WT5B	AGGGAGTCCACACAGGAAGACACG	12372-12349a	Exon 45	
Primers f	for genomic DNA amplification			
SI9.2F	CGGGCCTCTCGCTGCCTCTGCTCACCTCG	50143-50171b	Exon 42	563-758¢
SI9.2B	ACGGACCACTGGCGCACGAAGCGTAGCTG	50822-50794b	Exon 44	
SI9.3F	CGGCCTCGCTGCTCTTCCTGCTTTTGGTC	50678-50706b	Exon 43	145
S19.2B	ACGGACCACTGGCGCACGAAGCGTAGCTG	50822-50794b	Exon 44	

^aThe nucleotide positions are according to HUMPKD1A, GenBank Accession No. L33243(11).

The nested PCR product, amplified with S19F/S19B, was digested with either Taq I plus Bgl I or Pvu II (New England Biolabs) for detailed analysis of cDNA deletion observed.

Amplification of Genomic DNA

Genomic DNA samples were amplified in a total volume of 25 μl containing 200 ng of genomic DNA, 400 nM of each primer (Table 1), 200 μM dNTP mixture, 10 mM Tris-HCl (pH 8.3), 50 mM KCl, 1.25 unit AmpliTaqGold™ (PE Applied Biosystems), 5 per cent DMSO, and 1.0 mM MgCl₂. The PCR was initiated at 95°C for 10 min, then conducted for 2 cycles at 94°C for 30 s, 62°C for 30 s, and 72°C for 30-60 s (depended on size of PCR product). It was then continued for 31 cycles with 2°C reduction of annealing temperature every 2 cycles until reaching the final annealing temperature at 48°C, followed by a terminal extension at 72°C for 10 min.

DNA Sequencing

The PCR product, separated on agarose-gel electrophoresis, was purified using QIAquick™ Gel Extraction Kit (QIAGEN). The purified DNA frag-

ment was sequenced using ABI PRISM™ BigDye™ Terminator Cycle Sequencing Ready Reaction Kit and ABI PRISM 310 Automated DNA Sequencer (PE Applied Biosystems).

RESULTS

Linkage Analysis

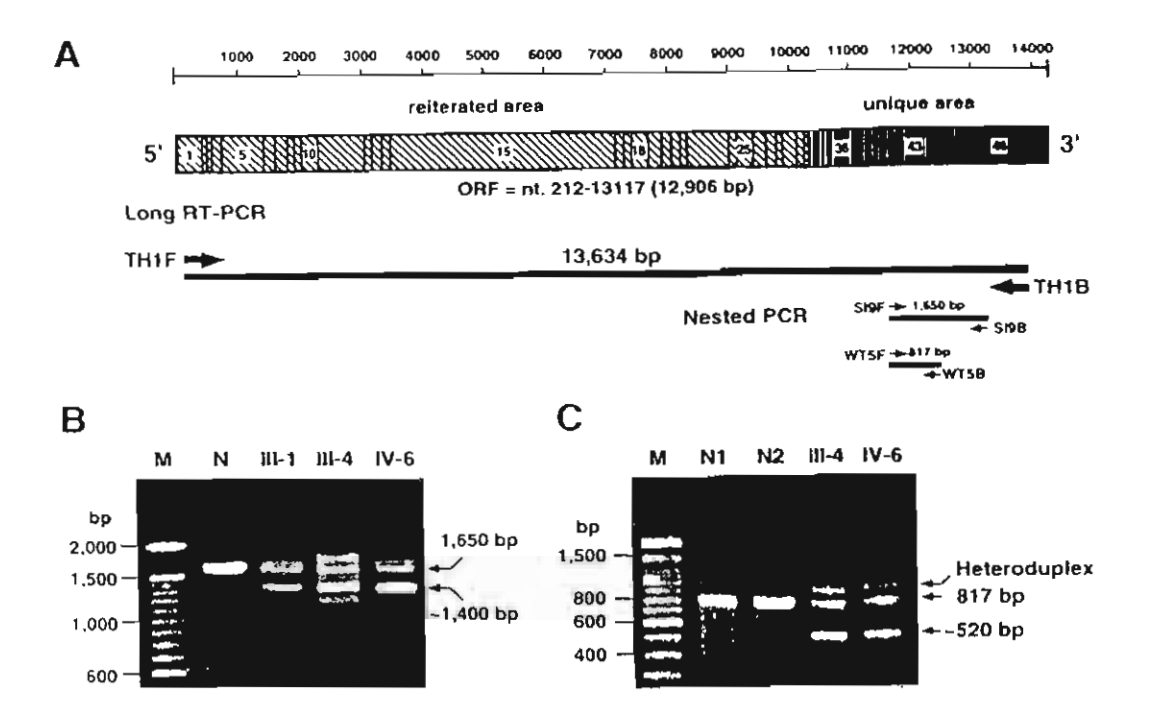
From analyses of five polymorphic DNA markers in the *PKD1* region on chromosome 16p, 14 haplotypes (with 5 additional variants) were found to segregate in PK009 family and the abnormal *PKD1* allele was linked to haplotype A, which consisted of the following alleles: 2.1 kb for D16S85, 123 bp for KG8, 110 bp for SM6, 169 bp for 16AC2.5, and 88 bp for SM7 (Fig. 3).

Long RT-PCR and Nested PCR

Long RT-PCR and nested PCRs were applied to RNA samples prepared from three affected members (III-1, III-4, and IV-6) of PK009 family, the results of which were mostly normal. However, with nested PCR using SI19F/SI19B primer pair, while a single PCR product (1,650 bp) was observed in samples from normal individuals, products with two different sizes, normal (1,650 bp) and

bThe nucleotide positions are according to HUMPKD1GEN, GenBank Accession No. L39891(10).

cSize of PCR product is variable due to numbers of variable repeated sequences in intron 42(14).



(A) Diagrammatic representation of the full-length PKD1 mRNA (upper), long PCR product (middle), Fig. 1. and nested PCR products (lower). The reiterated region in the PKD1 mRNA (exons 1-32) is represented by the hatched area and the unique region (exons 33-46) by the blackened area. Sizes (in bp) and primer pairs (arrows) are shown above and below the long RT-PCR products (long solid horizontal line) and nested PCR products (short solid horizontal lines), respectively. (B) Nested PCR products amplified from long PCR product of PKD1-cDNA with the SI9F/SI9B primers from a normal individual (N) and three PKD1 patients (III-1, III-4, and IV-6) of PK009 family. A single normal PCR product (1,650 bp) was observed in the normal sample while a normal and a shorter (~1,400 bp) products were found in three patients' samples. The uppermost band in the lanes of patients' samples is probably a heteroduplex of the normal and shorter products. Lane M is 100-bp DNA ladder. (C) Nested PCR products amplified from the long PKD1-cDNA samples by WT5F/WT5B primers of two normal individuals (N1 and N2) and the two patients (III-4 and IV-6) of PK009 family. A normal PCR product with the size of 817 bp was observed in the two normal samples but a normal (817 bp) and a shorter (~520 bp) fragments were detected in both patients' samples; the top band in both patients' samples was probably a heteroduplex of the normal and deleted DNA strands. Lane M is 100-bp DNA ladder.

shorter (~1,400 bp), were detected in samples from the three affected members (Fig. 1B). In addition, an upper and fainter band of PCR product was also noticed. The presence of a shorter product may have resulted from a partial deletion of PKD1 cDNA prepared from its mRNA transcript from one allele of PKD1 in these patients, and upper band might be a heteroduplex of the normal and deleted DNA strands.

To locate the region with possible deletion, nested PCR products amplified by SI9F/SI9B primer pair from a normal individual and a patient (III-4) were digested with either Taq I plus Bgl I or Pvu II. It was found that the deleted region was of 300 bp, located between the first Taq I and Bgl I sites (or the fourth site of Pvu II) (data not shown).

A new pair of primers (WT5F/WT5B; Table I and Fig. 1A) were designed to amplify DNA covering the deleted region. The result of the amplifications showed that two normal samples (N1 and N2) generated a single amplified product with the size of 817 bp, whereas, two patients' sam-

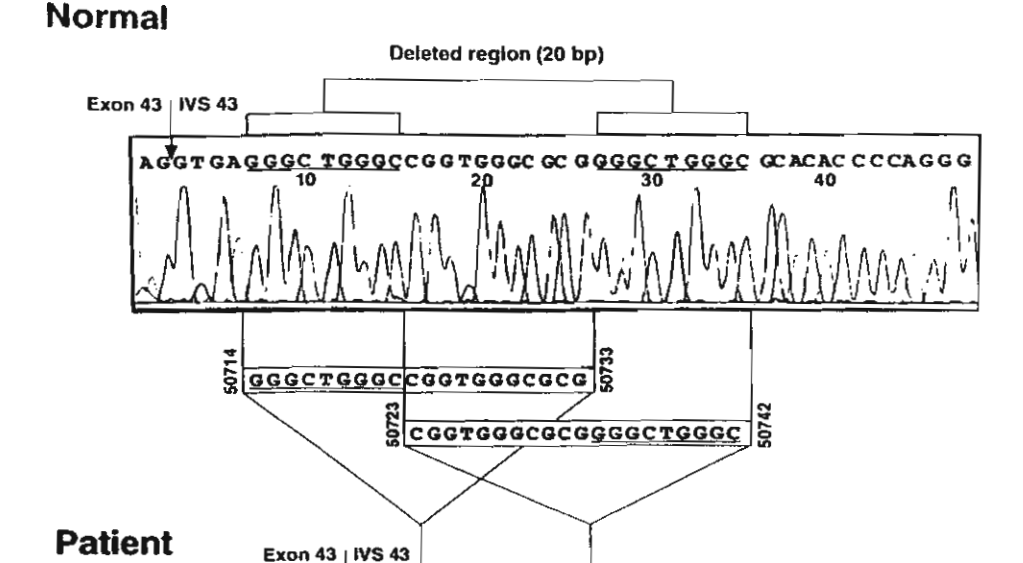


Fig. 2. Results of sequencing analyses of nested PCR products of intron 43 region amplified from genomic DNA samples of a normal control and patient III-4 of PK009 family by SI9.2F/SI9.2B primers. Comparison of the two nucleotide sequences shows a deletion of 20 bp in intron 43. The presence of two direct 9-nt repeat (GGGCTGGGC) (underlined) which are separated by 11 bp in the normal sequence of this intron makes many possibilities of the deletion breakpoint between the nucleotide positions 50714 and 50742 of PKD1 (GenBank Accession No. L39891). Two examples of possibilities of the 20-bp deletion at the most 5' and 3' ends are shown.

ples (III-4 and IV-6) produced the normal amplified product (817 bp) and a shorter fragment (~520 bp) together with the upper heteroduplex band (Fig. 1C).

Sequencing Analysis of the Shorter Nested-PCR Product

The 520 bp fragment was purified from agarose-gel electrophoresis and subjected to direct DNA sequencing. There was a deletion of 291 bp which corresponded to the total exon 43 sequence of *PKD1* while complete sequences of exons 42 and 44 were still present (data not shown). This finding indicated that the deletion was most likely due to the skipping of exon 43 from the *PKD1*-mRNA transcript.

Analysis of the PKD1 Gene

The skipping of exon 43 from *PKD1*-mRNA transcript might have occurred from a number of defects in the *PKD1* gene, viz. complete absence of the exon, mutation at the exon-intron junctions, or mutation at the A branch site in the flanking introns 42 and 43. To identify the precise mutation, genomic DNA in this region of *PKD1* was sequenced. Since the genomic region surrounding exon 43 was difficult to amplify by PCR due to the presence of 34-nt repeat polymorphism in intron 42(14), the primary genomic DNA amplification was performed by using SI9F/SI9B primer pair which had been used for nested PCR of *PKD1* cDNA (Table 1). A PCR product with the length of 2,351-2,546 bp was produced and used in nested PCR with SI9.2F/SI9.2B

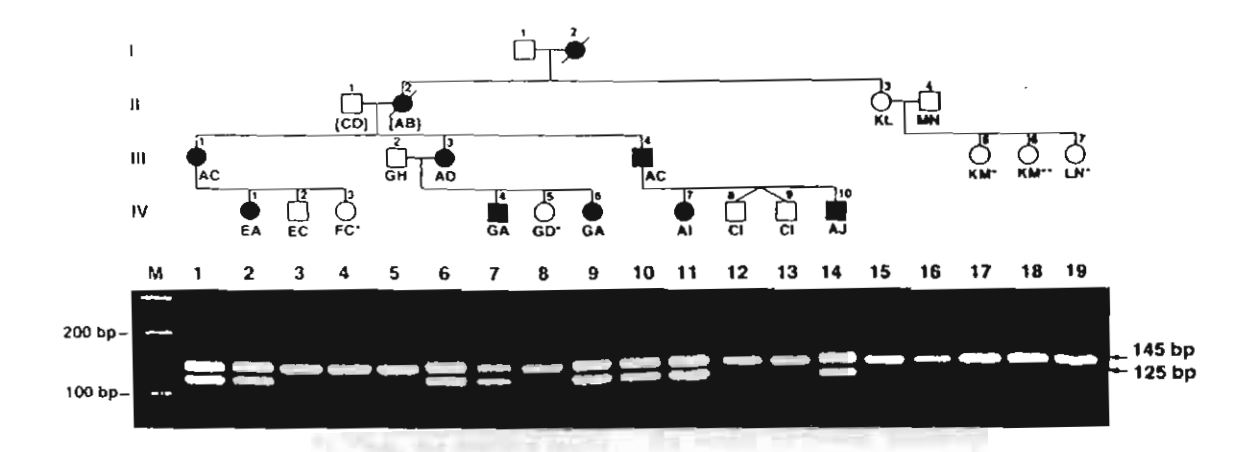


Fig. 3. Detection of the 20-bp deletion in intron 43 of PKD1 by amplification of genomic DNA samples from members of PK009 family with SI9.3F/SI9.2B primers. Pedigree of the family is shown and haplotyes in the region of PKD1 on chromosome 16p13.3, determined by using 5 polymorphic DNA markers, are indicated under the symbols. Genomic DNA samples from 19 family members, 8 from affected (filled symbols) and 11 from unaffected (blank symbols) members, were analyzed. DNA samples of the unaffected members produced only the product of the wild-type allele (145 bp) but those of affected members generated the products of both wild-type and mutant (125 bp) alleles. The mutant allele segregated with the haplotype A in the family. The haplotypes with one or two asterisks are variants of the ones without. Lane M is 100-bp DNA ladder.

primer pair'specific to sequences in exons 42 and 44 (Table 1). A PCR product with the size of 563-758 bp was generated and sequenced. There was a deletion of 20 bp in intron 43 (Fig. 2), while sequences in other regions were normal. Since there are two 9-bp repeats (GGGCTGGGC) situated 11 bp apart in intron 43 of PKD1, it was not possible to locate precisely the deletion breakpoints in this abnormal gene.

Direct Detection of the 20-bp Deletion in Intron 43 in Members of PK009 Family

To perform direct detection of the 20-bp deletion in intron 43 in members of PK009 family, a primer specific to the sequence of exon 43 (SI9.3F) was used together with a primer specific to the sequence of exon 44 (SI9.2B) (Table 1). With this primer pair, genomic DNA sample with normal intron 43 would generate PCR product of 145 bp while that with deleted intron 43 of 125 bp. When genomic DNA samples from all members of PK009 family were amplified, DNA samples of 11 normal members showed only the normal size product (145 bp), whereas, those of 8 affected members displayed 145

bp and 125 bp products (Fig. 3). Heteroduplex band was sometimes observed. The presence of deleted intron 43 in affected members and its absence in unaffected members of PK009 family corresponded with the presence and absence of haplotype A which linked to the abnormal *PKD1* allele (Fig. 3).

DISCUSSION

An analysis of PKD1-mRNA transcripts from three patients in PK009 family showed that the truncated PKD1 cDNA observed in the initial nested PCR screening (Fig. 1B and C) was due to skipping of the entire 291 nt sequence of exon 43, while the sequences of exon 42 and 44 were still intact in the abnormal transcript. Further analysis of PKD1-genomic DNA by direct sequencing revealed a 20-bp deletion in intron 43 of the patient's PKD1 gene (Fig. 2) while the sequences of other critical regions, such as splice donor and acceptor sites close to exon 43 and branch sites in the flanking introns, were not changed. Thus, the observed 20-bp deletion in intron 43 was most likely to be the cause of exon 43 skipping in the patient's mRNA transcript. A PCR method for amplification of DNA region covering

intron 43 was used to examine the deletion in DNA samples from 19 members of PK009 family. The expected 20-bp deletion in intron 43 was found in all samples from 8 affected members but was not detected in the 11 unaffected members (Fig. 3). In addition, the deletion segregated in complete linkage to the haplotype A as characterized by using 5 polymorphic DNA markers in the *PKD1* region (Fig. 3). All the evidence clearly supported the 20-bp deletion in intron 43 of *PKD1* as being the disease mutation in this family.

Two 9 bp direct-repeat sequences (GGGC TGGGC) separated by 11 nucleotides were present in *PKD1* intron 43 (Fig. 2). Thus, the deletion might have occurred from a misalignment between the two direct repeat sequences in this region of two *PKD1* alleles and interchromosomal recombination during meiosis. Since the length of deleted nucleotides (20 bp) was equal to the sum of one repeat (9 bp) and the joining part (11 bp), and one repeat sequence still remained in the deleted allele, the exact position of the recombination or deletion breakpoint could not be determined. As the deletion did not involve the nearby exon, it would not be detected by exon analysis of genomic DNA.

Mutations causing exon skipping usually involve either splice donor or splice acceptor site at 3' and 5' consensus sequences of the intron. Two reported mutations of *PKD1* resulting in exon 39 and exon 44 skipping are IVS39+1G>C and IVS44+1G>C substitutions, respectively(9,24). However, the intron 43 deletion leading to exon skipping reported here did not affect those functionally important sites. One explanation for the 20 bp-deletion in intron 43 causing exon 43 skipping may be that the truncated intron is too short for proper spliceosome formation and correct RNA splicing process. The minimal length of intron in human genes for correct *in vivo* splicing is not known. In an *in vitro* study to determine a minimal intron length using rabbit beta-

globin gene constructs in HeLa cells, it was found that the correct splicing required six 5' and twelve or more 3' intron nucleotides with at least 80 inner nucleotides (25). The shortest *PKD1* intron is intron 19 with a length of 66 bp(11). The length of the mutated intron 43 is 55 bp.

Deletions of 18 and 20 bp in intron 43 of *PKD1* have been reported(26). In each case, two different transcripts, either with deleted-intron sequence retained or with a 66-nt deletion due to activation of a cryptic 5' splice site, as well as the transcripts with exon 43 skipping, were produced. These findings are different from this study where the major defective transcript contained exon 43 skipping. It should be noted that in this study fresh peripheral blood lymphocytes were used for RNA isolation while lymphoblastoid cell lines were used in the previous work.

The deletion of 291 nucleotides of exon 43 in *PKD1*-mRNA transcript will lead to an in-frame deletion of 97 amino acids at positions 3904-4001 in polycystin-1. This deleted peptide region is located between the second half of the 7th transmembrane (TM) domain and the first one-third of the 9th TM domain of the proposed model of polycystin-1(27). Since the deletion of this region has resulted in the disease phenotype, it is of importance to the function of polycystin-1.

ACKNOWLEDGEMENTS

The authors thank the patients and family members for participation and donation of blood samples for the studies. We also thank Dr. Prida Malasit, Head of Division of Medical Molecular Biology, Department of Research and Development, for laboratory facilities, and staff of Renal Unit, Department of Medicine, Faculty of Medicine Siriraj Hospital for collection of blood samples. This work was partly supported by a grant from the Faculty of Medicine Siriraj Hospital. P.W. is also a Senior Research Scholar of the Thailand Research Fund.

REFERENCES

- Dalgaard OZ. Bilateral polycystic disease of the kidneys: a follow-up of two hundred and eighty four patients and their families. Acta Med Scand 1957; 328: 1-255.
- Reeders ST, Breuning MH, Davies KE, et al. A highly polymorphic DNA marker linked to adult polycystic kidney disease on chromosome 16. Nature 1985; 317: 542-4.
- Kimberling WJ, Kumar S, Gabow PA, et al. Autosomal dominant polycystic kidney disease - localization of the second gene to chromosome 4q13q23. Genomics 1993; 18: 467-72.
- Daoust MC, Reynolds DM, Bichet DG, et al. Evidence for a third genetic locus for autosomal dominant polycystic kidney disease. Genomics 1995; 25: 733-6.
- Peters DJM, Sandkuijl LA. Genetic heterogeneity of polycystic kidney disease in Europe. Contrib Nephrol 1992; 97: 128-39.
- Ravine D, Walker RG, Gibson RN, et al. Phenotype and genotype heterogeneity in autosomal dominant polycystic kidney disease. Lancet 1992; 340: 1330-3.
- Qian F, Watnick TJ, Onuchic LF, et al. The molecular basis of focal cyst formation in human autosomal dominant polycystic kidney disease type 1. Cell 1996; 87: 979-87.
- Brasier JL, Henske EP. Loss of the polycystic kidney disease (PKD1) region of chromosome 16p13 in renal cyst cells supports a loss-of-function model for cyst pathogenesis. J Clin Invest 1997; 99: 194-9.
- The European Polycystic Kidney Disease Consortium. The polycystic kidney disease 1 gene encodes a 14 kb transcript and lies within a duplicated region on chromosome 16. Cell 1994; 77: 881-94.
- Burn TC, Connors TD, Dackowski WR, et al. Analysis of the genomic sequence for the autosomal dominant polycystic kidney disease (PKD1) gene predicts the presence of a leucine-rich repeat. The American PKD1 Consortium (APKD1 Consortium). Hum Mol Genet 1995; 4: 575-82.
- Hughes J, Ward CJ, Peral B, et al. The polycystic kidney disease 1 (PKD1) gene encodes a novel protein with multiple cell recognition domains. Nat Genet 1995; 10: 151-60.
- The International Polycystic Kidney Disease Consortium. Polycystic kidney disease: the complete structure of the PKD1 gene and its protein. Cell 1995; 81: 289-98.
- Roelfsema JH, Spruit L, Saris JJ, et al. Mutation detection in the repeated part of the PKD1 gene. Am J Hum Genet 1997; 61: 1044-52.
- Peral B, Sanmillan JL, Ong ACM, et al. Screening

- the 3' region of the polycystic kidney disease I (PKD1) gene reveals six novel mutations. Am J Hum Genet 1996; 58: 86-96.
- Badenas C, Torra R, San Millan J, et al. Mutational analysis within the 3' region of the PKD1 gene. Kidney Int 1999; 55: 1225-33.
- The Human Gene Mutation Database at the Institute of Medical Genetics in Cardiff, URL: http://www.uwcm.ac.uk/uwcm/mg/search/120293.html (for PKD1).
- 17. Thongnoppakhun W, Wilairat P, Vareesangthip K, et al. Long RT-PCR amplification of the entire coding sequence of the polycystic kidney disease 1 (PKD1) gene. BioTechniques 1999; 26: 126-32.
- Bear JC, McManamon P, Morgan J, et al. Age at clinical onset and at ultrasonographic deletion of adult polycystic kidney disease: data for genetic couselling. Am J Med Genet 1984; 18: 45-53.
- Sambrook J, Fritsch EF, Maniatis T. Molecular cloning: a laboratory manual. 2nd ed. New York: Cold Spring Harbor Laboratory Press; 1989.
- Harris PC, Thomas S, Ratcliffe PJ, et al. Rapid genetic analysis of families with polycystic kidney disease 1 by means of a microsatellite marker. Lancet 1991; 338: 1484-7.
- Thompson AD, Shen Y, Holman K, et al. Isolation and characterisation of (AC)n microsatellite genetic markers from human chromosome 16. Genomics 1992; 13: 402-8.
- Germino GG, Somlo S, Weinstat-Saslow D, et al. Positional cloning approach to the dominant polycystic kidney disease gene, PKD1. Kidney Int 1993; 39 (Suppl): \$20-5.
- Peral B, Ward CJ, Sanmillan JL, et al. Evidence of linkage disequilibrium in the spanish polycystic kidney disease 1 population. Am J Hum Genet 1994; 54: 899-908.
- Peral B, Gamble V, Strong C, et al. Identification of mutations in the duplicated region of the polycystic kidney disease 1 gene (PKD1) by a novel approach. Am J Hum Genet 1997; 60: 1399-410.
- Wieringa B, Hofer E, Weissmann C. A minimal intron length but no specific internal sequence is required for splicing the large rabbit beta-globin intron. Cell 1984; 37: 915-25.
- Peral B, Gamble V, Millan JLS, et al. Splicing mutations of the polycystic kidney disease 1 (PKD1) gene induced by intronic deletion. Hum Mol Genet 1995; 4: 569-74.
- Sandford R, Sgotto B, Aparicio S, et al. Comparative analysis of the polycystic kidney disease 1 (PKD1) gene reveals an integral membrane glycoprotein with multiple evolutionary conserved domains. Hum Mol Genet 1997; 6: 1483-9.

ความผิดปกติของยืน *PKD1* ที่ทำให้เกิดความผิดปกติในกระบวนการตัดต่อ อาร์เอ็นเอในครอบครัวผู้ป่วยไทย

นัญวรรณ รุ่งโรจน์, วท.ม.*, วรรณา ทองนพคุณ, ปร.ด.*, เกรียงศักดิ์ วารีแสงทิพย์, พ.บ., Ph.D.**, จินตนา ศิรินาวิน, พ.บ.*,***, ประพนธ์ วิไลรัตน์, Ph.D.****, เพทาย เย็นจิตโสมนัส, Ph.D.*,*****

โรคไตเป็นถุงน้ำชนิต autosomal dominant มีสาเหตุใหญ่จากมิวเตชั่นของยืน PKD1 จากการศึกษา mRNA ของ ยืน PKD1 ด้วยวิธี long reverse transcription-polymerase chain reaction (RT-PCR) และ nested PCR คณะผู้วิจัยพบว่า PKD1-cDNA จากพี่น้อง 3 คน ที่เป็นโรคนี้จากครอบครัวเดียวกัน มีขนาดสั้นลงกว่าปกติประมาณ 250 คู่เบส การศึกษาใน รายละเอียดพบว่า PKD1-mRNA ของผู้ป่วยมีความผิดปกติในกระบวนการตัดต่ออาร์เอ็นเอ ทำให้ลำดับนิวคลีโอไทด์ของ exon 43 ซึ่งมีขนาด 291 นิวคลีโอไทด์ขาดหายไป คาดว่าทำให้ไปรดีน polycystin-1 ผิดปกติมีกรดอะมิโนหายไปจำนวน 97 ตัว ความผิดปกติในกระบวนการตัดต่ออาร์เอ็นเอในผู้ป่วยนี้ไม่ได้เกิดจากมิวเตชั่นที่ทำลาย splice donor หรือ acceptor site ที่อยู่ติดกับ exon 43 หรือ branch sites ใน intron ที่ขนาบข้าง แต่น่าจะเป็นผลจากการขาดหายของลำดับนิวคลีโอไทด์ จำนวน 20 คู่เบสใน intron 43 การขาดหายของดีเอ็นเอใน intron นี้ ตรวจพบในสมาชิกครอบครัวที่เป็นโรคจำนวน 8 คน แต่ไม่พบในผู้ที่ไม่เป็นโรค 11 คน ตรงกับผลการตรวจตัวยวิธี linkage analysis โดยใช้ polymorphic markers ในบริเวณ ใกล้ยุน PKD1 จำนวน 5 markers การวินิจฉัยโรคในครอบครัวนี้สามารถทำได้โดยตรงด้วยวิธี genomic DNA amplification เพื่อดรวจการขาดหายของดีเอ็นเอใน intron ของยืน PKD1

คำสำคัญ: ยีน Polycystic kidney disease 1 (*PKD1*), มิวเตชั่นของยีน *PKD1*, การขาดหายของอินทรอน, การข้ามเว้นของเอ็กซอน, ความผิดปกติในกระบวนการดัดต่ออาร์เอ็นเอ, การเชื่อมต่ออาร์เอ็นเอที่ผิดปกติ

นัญวรรณ รุ่งโรจน์, วรรณา ทองนพคุณ, เกรียงศักดิ์ วารีแสงทิพย์, จินตนา ศิรินาวิน, ประพนธ์ วิไลรัตน์, เพทาย เฮ็นจิตโสมนัส จดทมายเทตุทางแพทย์ ฯ 2544; 84: 1308–1316

- หน่วยอณพันธศาสตร์, สถานส่งเสริมการวิจัย, คณะแพทยศาสตร์ศิริราชพยาบาล,
- ** สาขาวิชาวักกะวิทยา, ภาควิชาอายุรศาสตร์, คณะแพทยศาสตร์ศิริราชพยาบาล,
- *** สาขาวิชาเวชพันธุศาสตร์, ภาควิชาอายุรศาสตร์, คณะแพทยศาสตร์ศิริราชพยาบาล,
- **** ภาควิชาชีวเคมี, คณะวิทยาศาสตร์, มหาวิทยาลัยมหิดล,
- ***** หน่วยอณูชีววิทยาการแพทย์, สถานส่งเสริมการวิจัย, คณะแพทยศาสตร์ศิริราชพยาบาล, มหาวิทยาลัยมหิดล, กรุงเทพฯ 10700

Active Site Contribution to Specificity of the Aspartic Proteases Plasmepsins I and II*

Received for publication, May 16, 2002, and in revised form, August 8, 2002 Published, JBC Papers in Press, August 19, 2002, DOI 10.1074/jbc.M204852200

Pilaiwan Siripurkpongts, Jirundon Yuvaniyamat, Prapon Wilairatt, Daniel E. Goldberg

From the ‡Department of Biochemistry, Faculty of Science, Mahidol University, Rama VI Road, Bangkok 10400, Thailand and ¶Howard Hughes Medical Institute, Departments of Molecular Microbiology and Medicine, Washington University School of Medicine, St. Louis, Missouri 63110

Plasmepsins I and II (PM I and II) are aspartic proteases involved in the initial steps of Plasmodium hemoglobin degradation. They are attractive targets for antimalarial drug development. The two enzymes are 73% identical, yet have different substrate and inhibitor specificities. The x-ray structures of proform and mature PM II have been determined, but models of PM I do not adequately explain the selectivity of the two proteases. To better understand the basis of these recognition differences, we have identified nine residues of PM II that are in proximity to the inhibitor pepstatin in the crystal structure and differ in PM L.We mutated these residues in PM II to the cognate amino acids of PM I. Kinetic parameters for substrate and inhibitors for the PM II-mutant were similar to those of PM II-wild type (WT). Cleavage specificity was assessed using hemoglobin or a random decamer peptide library as substrate. Again, PM II-mutant behaved like PM II-WT rather than PM I-WT. These results indicate that differences in plasmepsin specificity depend more on conformational differences from distant sites than on specific active site variation.

Malaria is a disease caused by parasites of the genus Plasmodium. The disease afflicts several hundred million and kills up to 3 million annually, mainly children (1). At the intraerythrocytic stage, these parasites consume hemoglobin as a major nutrient source for parasite growth and maturation. Hemoglobin degradation is mediated by the action of several digestive enzymes in the acidic food vacuole. Plasmepsins are aspartic proteases found in the food vacuole that are essential for degradation of hemoglobin. There appear to be four plasmepsins involved in hemoglobin degradation in the food vacuole of Plasmodium falciparum (2). PM I makes an initial cleavage at Phe-33-Leu-34 on the α -globin chain of hemoglobin (3), presumably leading to the unraveling of the hemoglobin molecule such that further proteolysis by PM II, PM IV, histoaspartic protease (HAP), falcipains, and facilysin can rapidly

proceed (2, 4-8). The small peptides formed from the action of these enzymes are converted to free amino acids by aminopeptidases and perhaps other enzymes (9, 10).

The World Health Organization has recognized the plasmepsins as attractive targets for the design of novel chemotherapeutic compounds for the treatment of malaria (11). The inhibition of their activities by peptidomimetic compounds specific for aspartic proteases results in death of the parasites (12–14). The elucidation of structure-activity relationships for these enzymes will facilitate the development of potent, specific inhibitors. Structures of PM II in both proforms and mature forms are available (15, 16). Unfortunately, the structure of PM I is still unknown, even though it is important in the first step of hemoglobin degradation. Active, recombinant PM I has been generated (13), but its limited yield and solubility have prevented its crystallization.

Based on the structure of PM II co-crystallized with pepstatin, a specific peptide inhibitor of aspartic proteases (15), amino acid residues in the active site of PM II in proximity to the pepstatin molecule were compared with the corresponding amino acids in PM I. Nine amino acids that differed between the two enzymes were chosen for site-directed mutagenesis. We hypothesized that putting these nine amino acid residues of PM I in the PM II scaffold structure would give rise to a specificity similar to that of PM I. We hoped that this approach would allow us to obtain a structure of the PM I active site on the soluble PM II structure core. Unexpectedly, our data show that engineering a PM II with the active site surface of PM I largely maintains the PM II substrate and inhibitor specificity.

EXPERIMENTAL PROCEDURES

Reagents—QuikChange™ site-directed mutagenesis kit was obtained from Stratagene (La Jolla, CA). Pepstatin A was obtained from ICN (Costa Mesa, CA). P1 inhibitor was obtained from J. Erickson, NCI-Frederick, MD. SC-50083 inhibitor was obtained from Searle Pharmaceuticals, St. Louis, MO. All other reagents were from Sigma. Plasmepsin I pET3a plasmids were obtained from Dr. Richard P. Moon (Hoffmann-La Roche).

Mutation Constructs—Based on the structure of PM II co-crystallized with pepstatin, nine amino acid residues were chosen for mutation. Using the QuikChangeTM site-directed mutagenesis kit following manufacturer's directions, mutations in the active site of the PM II gene were generated. Mutations were done in several steps using the different pairs of mutagenic primers encoding the amino acid residues in the active site of PM II to replace the amino acid residues in the active site of PM II.

The mutagenic primers encoded the target I14V and F16Y (5'-GAT-TTCCAAAATGTGATGTATTATGGTGATGCAGAAGTTGG-3', 5'-CAT-CACCATAATACATCACATTTTGGAAATCTACTAATTCG-3'), T114A (5'-CCAGAGTATACGCTGGTTCGAATCCATTAGTATC-3', 5'-GATTC-GAACCAGCGTATACTCTGGGCCAGTTTG-3'), A117L, S118G, and T119Q (5'-CCAAGGATACCATCAAACTGGCCCAGAGTATAAGTTGG-TTCGAATCC-3', 5'-CGAACCAACTTATACTCTGGGCCAGTTTGATG-GTATCCTTGGTTTTAGG-3'), A219S (5'-GTGGTACTAGTTCTATTACT-GTACCAACTGAC-3', 5'-GGTACAGTAATAGAACTAGTACCACTATC-GTACCAACTGAC-3', 5'-GGTACAGTAATAGAACTAGTACCACTATC-

^{*}This work was supported in part by TARUN Grant 00-2-MAL/TARUN-02-010 (to J. Y.), from the Thailand Tropical Diseases Research Program, the Senior Researcher Fellowship (to P. W.), from the Thailand Research Fund, and National Institutes of Health Grant AI-47798 (to D. E. G.). The costs of publication of this article were defrayed in part by the payment of page charges. This article must therefore be hereby marked "advertisement" in accordance with 18 U.S.C. Section 1734 solely to indicate this fact.

 $^{\ \}mbox{\it Recipient}$ of the Royal Golden Jubilee Fellowship from Thailand Research Fund.

[|] Recipient of the Burroughs Wellcome Fund Scholar Award in Molecular Parasitology. To whom correspondence should be addressed. Tel.: 314-362-1514; Fax: 314-367-3214; E-mail: goldberg@borcim. wustl edu.

TAC-3'), L292V and F294L (5'-TTGGTACTGGCAGATCCACTCCTAT-GATATTAAGCATAC-3', 5'-ATATCATAGGAGTGGATCTGCCAGTAC-CAACCTTTATTCTAG-3'). Plasmid DNA from mutants was sequenced to confirm that only the desired mutations were incorporated.

Expression and Purification of Recombinant Plasmepsins—The pET3a plasmids containing plasmepsin sequences were transformed into Escherichia coli BL21(DE3)pLysS. For PM II-WT and PM II-mutant, transformants were grown at 37 °C in LB broth containing 100 µg/ml ampicillin and 170 µg/ml chloramphenicol. At A_{noo} of 0.5, isopropyl-1-thio- β -D-galactopyranoside was added to 0.5 mm, and culture was grown at 37 °C for 5 h. For PM I-WT, transformants were cultured in super medium (25 g/liter bacto-tryptone; 15 g/liter bacto-yeast extract; 10 g/liter NaCl) containing 50 µg/ml ampicillin and 35 µg/ml of chloramphenicol. Upon reaching an A_{600} of 0.8, they were induced for 2 h by addition of 0.5 mm isopropyl-1-thio- β -D-galactopyranoside. After cells were harvested by centrifugation (5000 × g, 15 min, 4 °C) and lysed by sonication, protein expression was analyzed by using 12.5% SDS-PAGE.

For PM II-WT and II-mutant, the recombinant proplasmepsins were expressed as inclusion bodies, which were resuspended in 20 mm Tris-HCl, pH 7.4, 150 mm NaCl, 5 mm dithiothreitol (buffer A) and sequentially washed with: 1) 1% CHAPS1 in buffer A, twice; 2) 1 M NaCl in buffer A; 3) 1 M ures in buffer A, and 4) buffer A. The washed pellet was solubilized in 50 mm Tris buffer, pH 7.4, containing 6 m urea, 500 mm NaCl, 50 mm dithiothreitol, and 1 mm EDTA and then dialyzed in 50 mm Tris buffer, pH 7.4, containing 6 m urea, 50 mm dithiothreitol, and 1 mm EDTA (buffer B) overnight at 4 °C. The dialysate was applied to a mono-Q-Sepharose column (Amersham Biosciences). The column was eluted with a linear NaCl gradient (0-1 M in buffer B), and the fractions containing proplasmepsins, as analyzed by SDS-PAGE, were pooled and diluted with the same buffer to 1 mg/ml protein concentration. Refolding of proplasmepsins was initiated by stepwise dialysis for 4 h against five times the original volume of 20 mm Tris-HCl, pH 8.0, in Spectrapor dialysis tubing (MWCO 12-14 kDa) at 4 °C. The dialysis buffer was changed four times. The dialysate was centrifuged to remove any precipitate and applied to a mono-Q-Sepharose column (8 ml) equilibrated in 20 mм Tris, pH 8.0, buffer at 4 °C using an Amersham Biosciences FPLC. The column was eluted with a linear NaCl gradient (0-1 M) in the same buffer. The fractions containing proplasmepsins were pooled and stored at 4 °C.

For PM I-WT, the recombinant proplasmepsin (construct and basic procedure of Moon, Ref. 13) in inclusion bodies was resuspended in wash buffer (100 mm Tris-HCl, pH 8.0, 10% glycerol, 1 mm MgSO4, 150 mm NaCl, 0.1% Triton X-100, 5 mm EDTA containing protease inhibitor (e-aminocaproic acid) and benzonase (RNase and DNase)), and sequentially washed with: 1) 1% CHAPS in wash buffer, twice; 2) 0.5 M NaCl in wash buffer; 3) wash buffer; and 4) 2 M urea in wash buffer. The final washed pellet was solubilized in 50 ml of 8 m urea, 20 mm Tris-HCl, pH 8.0, and 1 mm EDTA containing protease inhibitors (c-aminocaproic acid and benzamidine-HCl). After centrifugation to remove the precipstate, the solution was dialyzed against 1 liter of Aq buffer (20 mm Tris-HCl, pH 8.0, 6 M urea, 1 mM EDTA) overnight at 4 °C and then applied to a mono-Q-Sepharose column (8 ml). The column was eluted with a linear NaCl gradient (0-1 M in Aq buffer), and the fractions containing PM I-WT, as analyzed by SDS-PAGE, were pooled and dialyzed against 1 liter of Aphos buffer (20 mm Tris-HCl, pH 8.0, 10% glycerol, 1 mm EDTA, and 6 m urea) overnight at 4 °C. The dialysate was applied onto a 1-ml heparin-Sepharose column (Amersham Biosciences) and cluted with a linear NaCl gradient (0-0.5 M) in Aphos buffer. Fractions containing PM I-WT were pooled, the protein concentration was determined, and the sample was diluted to 0.1 mg of protein/inl with Aphos buffer. Refolding of PM I-WT was done by stepwise dialysis. First, PM I-WT was dialyzed against 1 liter of refolding buffer 1 (25 mm glycylglycine, pH 9.5, 40 mm arginine, 0.5 m NaCl, 1 mm EDTA, 25% glycerol, 4 mm GSH and 0.4 mm GSSG) for 2 days at 10 °C with two buffer changes. Second, the solution was dialyzed against 1 liter of refolding buffer 2 (20 mm glycylglycine, pH 9.0, 25% glycerol, 0.15 M NaCl, 1 mm EDTA, 0.01% Triton X-100, 50 mm (NH₄)₂SO₄) for 2 days at 10 °C with two buffer changes. Protein was concentrated to 4 ml and dialyzed overnight at 4 °C against 500 ml of buffer containing 20 mm glycylglycine, pH 9.0, 5% glycerol, 1 mm EDTA, and 0.15 m NaCl.

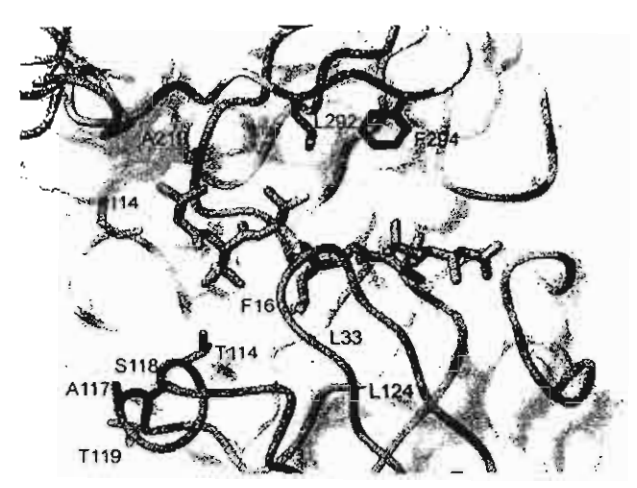


Fig. 1. Structure of PM II (PDB ID 1sme; Ref. 15) active site residues surrounding the inhibitor pepstatin (magenta). Amino acids in green are identical between PM I and PM II, whereas those in yellow and red are different. The PM II residues that were mutated to the corresponding residues of PM I in this work are shown in red. Leucines at positions 33 and 124 are not on the active site surface. They are more than 7 Å away and are not in direct contact with pepstatin. This figure was initially prepared with the program MOLMOL (24).

	PM II-WI		PM I	-WT	PM II mutant
97 66	M Pro Meture	м 	Pro	Mature	Pro Mature
43	-				Harris,
31					Recting a
21	-16/2				5240-
14					***

Fig. 2. Activation of plasmepsins upon lowering the pH to 5.0. Proform and mature form were analyzed by 12.5% SDS-PAGE.

PM 1-WT was concentrated and kept at $4\,^{\circ}\text{C}$ for further characterization.

Activation of Proplasmepsins—Prior to assay, the mature forms of plasmepsins were generated by adding one-tenth volume of 1 M sodium acetate. pH 5.0, for 24 h at room temperature. Autocatalytic processing of each zymogen (43 kDa) to mature form (37 kDa) was monitored by SDS-PAGE.

Determination of Plasmepsin Activity—The fluorogenic substrate used for the assay based on the sequence surrounding the Hb α Phe33-Leu34 initial cleavage site (3) was DABCYL-GABA-Glu-Arg-Met-Phe-Leu-Ser-Phe-Pro-GABA-EDANS. This peptide sequence is flanked by a fluorophore group, EDANS, and a quenching group, DABCYL (17). Fluorescence is quenched in the intact peptide, and quenching is relieved when the peptide is cleaved by enzyme.

The assay was performed in quartz cuvettes with a PerkinElmer Life Sciences LS50B fluorometer at an excitation wavelength of 336 nm, slit width of 5 nm, and emission wavelength of 490 nm, slit width of 10 nm at 37 °C with samples containing fluorogenic substrate, 100 mm sodium acetate, pH 5.0, 10% glycerol, and 0.01% Tween 20. K_m and $V_{\rm max}$ values were determined by measurement of initial velocities in duplicate or triplicate with at least six fluorogenic substrate concentrations. The $k_{\rm rnt}$ value was calculated from the following equation.

$$V_{\text{max}} = k_{\text{cnl}}[E]$$
 (Eq. 1)

For K_i determinations, inhibitors were equilibrated with enzyme at room temperature for 5 min followed by the addition of fluorogenic substrate stock. The change of fluorescence intensity was measured as a function of time. Assays were performed in duplicate or triplicate at five to six inhibitor concentrations for each K_i determination. Data were fitted by nonlinear regression analysis to the equation derived by Williams and Morrison (18).

¹ The abbreviations used are: CHAPS, 3-[(3-cholamidopropyl)dimethylammonio]-1-propanesulfonic acid; DABCYL, 4-(4-dimethylaminophenyl-azolbenzoic acid; GABA, γ-aminobutyric acid; EDANS, 5-((2-amino-ethyl)amino)naphthalene-1 sulfonic acid; HPLC, high pressure liquid chromatography; WT, wild type.

$$v/v_{o} = 1 - (|E| + |I| + K_{o}^{app}) - (|E| + |I| + K_{o}^{app})2 - 4|E|[I]2[E]$$
 (Eq. 2)

For competitive inhibitors:
$$K_{app}^{app} = K_{i}(1 + |SVK_{m})$$
 (Eq. 3)

The precise concentration of each PM II and I preparation was determined by active site titration with pepstatin as described previously (19, 20).

TABLE I

Kinetic parameters of plasmepsins using a fluorogenic substrate

DABCYL-GABA-Glu-Arg-Met-Phe*Leu-Ser-Phe-Pro-GABA-EDANS
(17). Initial rates were measured at 37 °C using 1-5 nM enzyme.

Plasmepsin	K_m	k _{ent}	k_{ent}/K_m
	μ×ι	sec-1	μ. sec - ^J
I-WT	0.917 ± 0.144	0.473 ± 0.172	0.528 ± 0.232
II-WT	0.489 ± 0.080	2.313 ± 0.092	4.813 ± 0.795
II-mutant	0.430 ± 0.064	2.206 ± 0.134	5.196 ± 0.718

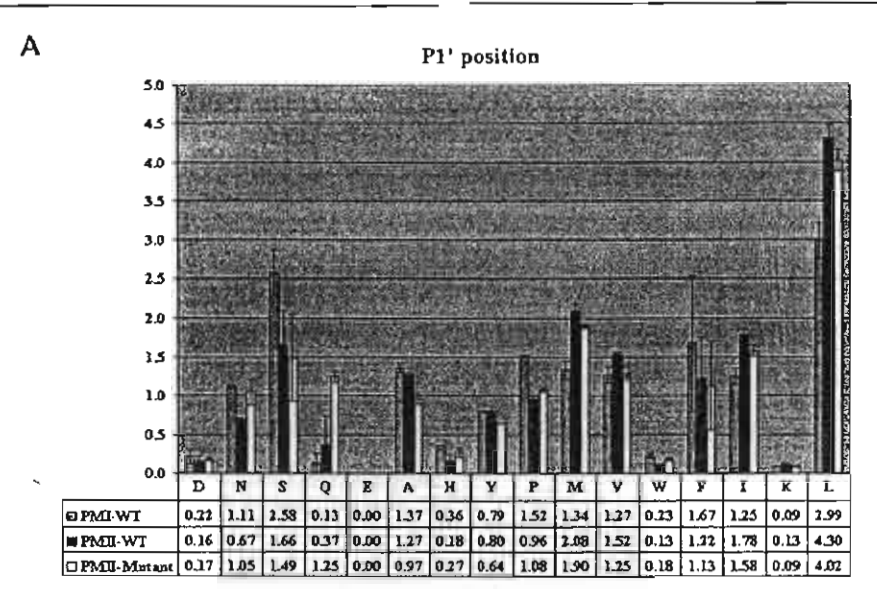
Hemoglobin Degradation—Human hemoglobin A (150 μ g) was incubated with PM J-WT, 11-WT, and II-mutant in 500 μ l of 100 mm sodium acetate, pH 5.0, 10% glycerol, and 0.01% Tween 20 at 37 °C for various

TABLE II

Inhibition of plasmepsins by peptidomimetic compounds

The fluorogenic substrate mentioned in Table I was used. For SC-50083, limited compound was available, so inhibition at a fixed substrate concentration (0.4 μm for PM II-WT and PM II-mutant; 0.8 μm for PM I-WT) and a varied inhibitor concentration was measured. Initial rates were determined at 37 °C using 0.3–5 nm enzyme.

Plasmepsin	K;-Pepstatin	IC ₅₀ - SC50083
	пы	j.M
I-WT	0.565 ± 0.224	0.132
II-WT	0.037 ± 0.010	3.467
II-mutant	0.061 ± 0.024	4.467



В

P2' position

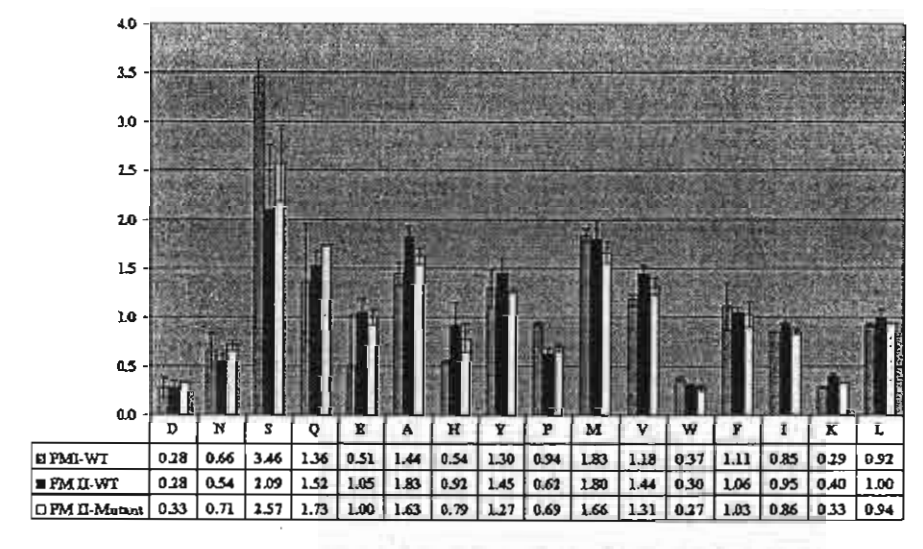


Fig. 3. Analysis of random 10-mer peptide cleavage by plasmepsins. A random peptide substrate was digested by PM I-WT, II-WT, and II-mutant at pH 5.0, 37 °C for 1 h. Cleavage preferences were analyzed by N-terminal amino acid sequencing. Data are normalized so that a value of 1 corresponds to the average quantity per amino acid in a given sequencing cycle. Because of interfering background peaks, glycine, threonine, and arginine could not be reliably quantitated and therefore were omitted.

times. The reaction was stopped by adding 100 μl of glacial acetic acid. The digest was subjected to reverse phase-HPLC using a RP-18 spheri-5 column, 1 mm \times 25 cm (Applied Biosystems) in mobile phase containing 0.1% trifluoroacetic acid with an accelerating (nonlinear) gradient of 18–60% acetonitrile at 80 μl min over 60 min and with detection at 214 mm.

Random Peptide Substrate and N-terminal Amino Acid Sequencing—A random peptide, acetyl-Xaa $_{10}$ -Lys(biotin) was synthesized, where X= all 20 amino acids except cysteine. 20 μm of random peptide substrate was incubated with PM I-WT, II-WT, and II-mutant in 100 mm sodium acetate, pH 5.0, 10% glycerol, and 0.01% Tween 20 at 37 °C for various times and heated to 100 °C for 5 min. The digest was sent for N-terminal amino acid sequencing. Amino acid preference in a given cycle was calculated by normalizing the amount of a particular residue to the average amount per amino acid residue in that cycle. Thus, a residue with an average quantity for that cycle has a value of 1. The data were corrected for bias present in the random peptide library by dividing each value by the relative amount of that particular amino acid in the starting mixture.

RESULTS

PM I and II are homologous, hemoglobin-degrading aspartic proteases. The mature enzyme sequences are 73% identical (85% homologous). Despite this, the two hydrolases display quite different substrate and inhibitor specificities. To better understand the basis for this difference, we examined the crystal structure of PM II bound to the inhibitor, pepstatin, and identified residues in the active site that are in contact with inhibitor. Nine such amino acids differ between PM I and PM II (Fig. 1). We changed all nine amino acids in the recombinant PM II background to the cognate residues found in PM I. We compared enzyme properties of the mutant PM II to those of wild-type PM I and II. Heterologous expression of recombinant PM I-WT, PM II-WT, and PM II-mutant yielded products of 43 kDa as determined by SDS-PAGE. Activation of these proplasmepsins by lowering the pH to 5 produced the 37-kDa mature forms (Fig. 2).

Table I shows the kinetic parameters of PM I-WT, PM II-WT, and PM II-mutant. Using a fluorogenic peptide based on the initial hemoglobin cleavage site, the $k_{\rm cat}$, K_m , and $k_{\rm cat}/K_m$ values were comparable for PM II-WT and PM II-mutant. In contrast, these values differed for PM I-WT; most dramatically, the PM I-WT specificity constant $(k_{\rm cat}/K_m)$ was about 10-fold lower than those of the PM II enzymes.

Table II shows an assessment of the ability of two different compounds to inhibit the plasmepsins. Similar K_i values were measured for PM II-WT and PM II-mutant with the tight binding inhibitor, pepstatin. PM I-WT had a K_i value an order of magnitude higher. Another inhibitor with differential ability to inhibit PM I and II was studied; because of limited compound availability, inhibition over a range of inhibitor concentration was measured at fixed substrate concentration to yield IC50 values. The IC50 of SC50083 for PM I-WT is 30-fold lower than that of PM II-WT. The IC50 of PM II-mutant is similar to that of PM II-WT.

We analyzed the ability of the three enzymes to cleave a random decamer peptide library. N-terminal amino acid sequencing was performed after a 1-h incubation to determine the amino acid preference on the P' side of the substrate (Fig. 3). Use of a similar dodecamer in other systems has been reported (21). The most dramatic preferences are seen at the P1' position, where PM II-WT and PM II-mutant both prefer leucine about 4-fold more than the average amino acid and methionine about 2-fold. PM I-WT has a similar specificity, with a slightly diminished preference for these two residues and an increased preference for serine at P1'. At P2', serine was preferred by each enzyme. At P3'-P5' (not shown, variance <2-fold), amino acid preferences are on a much smaller scale and are comparable among the three plasmepsins (data not shown). Similar results were obtained from 4-h and overnight

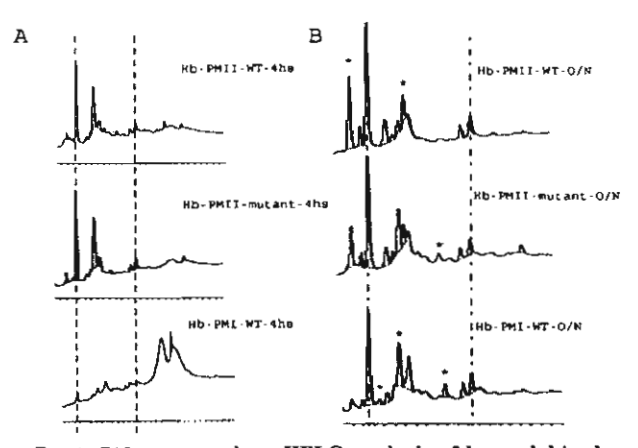


Fig. 4. C18 reverse phase-HPLC analysis of hemoglobin degradation products. Hemoglobin A was digested with PM I-WT, II-WT, and II-mutant at pH 5.0, 37 °C for 4 h (A) and 15 h (B). The digest was fractionated by HPLC using an RP-18 column with an acetonitrile gradient. * denotes peak that varies significantly between profiles at 15 h.

incubations of the random peptide substrate with each plasmepsin (data not shown).

To extend the results beyond use of peptides and peptide-like compounds, the natural substrate hemoglobin was incubated with each of the three enzymes. Fig. 4 shows the C18-reverse phase HPLC elution profile of peptide products. For a 4-h incubation, the PM II-mutant profile is similar to PM II-WT profile, but the PM I-WT profile is different. For overnight incubation, there are five major peaks of peptide products that differ between wild-type PM I and II. The PM II-mutant profile shares the PM II-WT profile at four of these sites.

DISCUSSION

PM I and II are highly homologous enzymes but have different affinities for substrates and inhibitors. We have mutated the PM II active site so that its surface mimics that of PM I. Surprisingly, the enzyme specificity is essentially unchanged from the parent enzyme. Based on the PM II crystal structure, Silva et al. (15) suggested three amino acids that vary between PM I and II that might be important in selectivity: Thr-114, Leu-292, Phe-294. Our PM II-mutant includes these three changes, yet specificity was not altered. In some aspartic proteases, the polyproline loop can have interactions with substrate. This loop is divergent between the two plasmepsins. However, a swap of PM I and II loops has been carried out without effect on specificity (17). Consistent with this, the loop does not appear to contact pepstatin in the crystal structure of PM II (15). Although the high similarity of the two enzymes suggests the same overall folding topology, our findings indicated that there must be sufficient structural differences other than active site residues that influence selectivity of the plasmepsins.

The proform and mature form of PM II may be regarded as two proteins with the same active site residues but different activity. Khan et al. (22) have shown that this activity disparity is a result of alteration in active site conformation and not of active site blockage. Upon enzyme activation, the conformational change leads to the formation of a functional PM II active site (22). For the case of PM I and PM II, it is possible that amino acid residues further away from the active site might cause some differences in their active site conformation and hence the differences in enzyme activity. The implication of our results is that differences in amino acid residues distant from the active site may play a significant role in determining spec-

ificity differences between two similar enzymes.

Interestingly, the most dramatic range of PM II amino acid preference in the random peptide analysis was seen at the P1' position. This position has not been extensively evaluated in other assays where the P1' residue was fixed as a chromogenic reporter. As would be expected from previous analysis of globin cleavage sites (6), PM II strongly preferred hydrophobic amino acids at the P1' site. Proline was also accepted at this position, as is the case for the human immunodeficiency virus protease (23). The P1' preference for leucine over the least favored amino acids was >50-fold. In contrast, at each of the other positions (P2'-P5'), all amino acids were tolerated within a 7-fold range.

This work gives us insight into the importance of the overall fold of a protein molecule on substrate specificity. Even in quite similar proteins, the geometry of the active site, not just the surface side chains, can be different enough to affect specificity. We have much to learn about the PM I active site that can not be gleaned from homology modeling.

Acknowledgments-We thank Dr. Richard P. Moon for the plasmepsin I clone, Dr. Bela Tackac for the plasmepsin I purification protocol, Dr. Porntip Petmitr for FPLC facilities, Dr. Dave McCourt for Nterminal amino acid sequencing, and Dr. Eva Istvan for critical review of this manuscript.

REFERENCES

- Trigg, P. I., and Kondrachine, A. V. (1998) Bull. W.H.O. 76, 11-16
 Banerjee, R., Liu, J., Beatty, W., Pelosof, L., Klemba, M., and Goldberg, D. E. (2002) Proc. Natl. Acad. Sci. U. S. A. 99, 990-995
- (2002) Proc. Natl. Acad. Sci. U. S. A. 99, 990-995
 3. Goldberg, D. E., Slater, A. F., Beavis, R., Chait, B., Cerami, A., and Henderson, G. B. (1991) J. Exp. Med. 173, 961-969
 4. Goldberg, D. E. (1992) Infect. Agents Dis. 1, 207-211
 5. Francis, S. E., Gluzman, I. Y., Oksman, A., Banerjee, D., and Goldberg, D. E.

- (1996) Mol Biochem, Parasitol, 83, 189-200.
- Gluzman, I. Y., Francis, S. E., Oksman, A., Smith, C. E., Duffin, K. L., and Goldberg, D. E. (1994) J. Clin. Invest. 93, 1602–1608
 Eggleson, K. K., Duffin, K. L., and Goldberg, D. E. (1999) J. Biol. Chem. 274, 32411–32417
- Dame, J. B., Reddy, G. R., Yowell, C. A., Dunn, B. M., Kay, J., and Berry, C.
- (1994) Mol. Biochem. Parasitol. 64, 177-190 Kolakovich, K. A., Gluzman, I. Y., Duffin, K. L., and Goldberg, D. E. (1997) Mol. Biochem. Parasitol. 87, 123-135
- 10. Gavigan, C. S., Dalton, J. P., and Bell, A. (2001) Mol. Biochem. Parasitol. 117, 37-48
- Coombs, G. H., Goldberg, D. E., Klemba, M., Berry, C., Kay, J., and Mottram, J. C. (2001) Trends Parasitol. 17, 532-537
- Francis, S. E., Gluzman, I. Y., Olsaman, A., Knickerbocker, A., Mueller, R., Bryant, M. L., Sherman, D. R., Russell, D. G., and Goldberg, D. E. (1994) EMBO J. 13, 306-317
- 13. Moon, R. P., Tyas, L., Certa, U., Rupp, K., Bur, D., Jacquet, C., Matile, H.,
- Hour, H., Grueninger-Leitch, F., Kay, J., Dunn, B. M., Berry, C., and Ridley, R. G. (1997) Eur. J. Biochem. 244, 552-560
 Haque, T. S., Skillman, A. G., Lee, C. E., Habashita, H., Gluzman, I. Y., Ewing, T. J., Goldberg, D. E., Kuntz, I. D., and Ellman, J. A. (1999) J. Med. Chem. 42, 1428-1440
- Silva, A. M., Lee, A. Y., Gulnik, S. V., Maier, P., Collins, J., Bhat, T. N., Collins, P. J., Cachau, R. E., Luker, K. E., Gluzman, I. Y., Francis, S. E., Oksman, A., Goldberg, D. E., and Erickson, J. W. (1996) Proc. Natt. Acad. Sci.
- U. S. A. 93, 10034 10039
 16. Bernstein, N. K., Cherney, M. M., Loetscher, H., Ridley, R. G., and James

- Bernstein, N. K., Cherney, M. M., Loetscher, H., Ridley, R. G., and James, M. N. (1999) Nat. Struct. Biol. 6, 32-37
 Euker, K. E., Francis, S. E., Gluzman, I. Y., and Goldberg, D. E. (1996) Mol. Biochem. Parasitol. 79, 71-78
 Williams, J. W., and Morrison, J. F. (1979) Methods Enzymol. 63, 437-467
 Knight, C. G. (1995) Methods Enzymol. 248, 85-101
 Copeland, R. A. (2000) Enzymes: a Practical Introduction to Structure, Mechanism, and Data Analysis, 2nd, Ed., Wiley-VCH, Inc., New York, NY
- 21. Turk, B. E., Huang, L. L., Piro, E. T., and Cantley, L. C (2001) Nat. Biotechnol. 19, 661-667
- Khan, A. R., Khazanovich-Bernstein, N., Bergmann, E. M., and James, M. N. (1999) Proc. Natl. Acad. Sci. U. S. A. 96, 10968-10975
- Poorman, R. A., Tomasselli, A. G., Heinrikson, R. L., and Kezdy, F. J. (1991) J. Biol. Chem. 266, 14554-14561
- 24. Koradi, R., Billeter, M., and Wuthrich, K. (1996) J. Mol. Graph. 14, 51-55.
- 29 32



Parasitology International 51 (2002) 99-103



Research note

Stage specificity of *Plasmodium falciparum* telomerase and its inhibition by berberine

N. Sriwilaijareon^a, S. Petmitr^b, A. Mutirangura^c, M. Ponglikitmongkol^a, P. Wilairat^{a,*}

^a Department of Biochemistry, Faculty of Science, Mahidol University, Rama 6 Road, Bangkok 10400, Thailand Department of Tropical Nutrition and Food Science, Faculty of Tropical Medicine, Mahidol University, Bangkok 10400, Thailand

^cDepartment of Anatomy, Faculty of Medicine, Chulalongkorn University, Bangkok 10400, Thailand

Received 26 February 2001; accepted 21 September 2001

Abstract

Telomerase activity in synchronized *Plasmodium falciparum* during its erythrocytic cycle was examined using the TRAP assay. Telomerase activity was detected at all stages of the parasite intraerythrocyte development, with higher activity in trophozoite and schizont stages compared with ring form. Berberine, extracted from *Arcangelisia flava* (L.) Merr., inhibited telomerase activity in a dose-dependent manner over a range of 30-300 μ M, indicating that *P. falciparum* telomerase might be a potential target for future malaria chemotherapy. © 2002 Elsevier Science Ireland Ltd. All rights reserved.

Keywords: Plasmodium falciparum; Telomerase; Berberine; Antimalarial

Telomeres, the ends of linear chromosomes, preserve genome stability and cell viability by preventing aberrant recombination and degrada-

tion of DNA [1]. Telomerase, a ribonucleoprotein enzyme, functions to elongate telomeres and cells that fail to activate telomerase cannot compensate for the end replication problem. Consequently, these cells have a limited number of cell divisions [2]. Telomerase activity has been reported in the human malaria parasite, *Plasmodium falciparum*, [3] with the most pronounced

E-mail address: scpwl@mahidol.ac.th (P. Wilairat).

 $\frac{133}{3}$ -5769/02/\$ - see front matter © 2002 Elsevier Science Ireland Ltd. All rights reserved. FII: $\frac{5}{3}$ 1 3 8 3 - 5 7 6 9 (0 1) 0 0 0 9 2 - 7

^{*} Corresponding author. Tel: +66-2-2455-195; fax: +66-2-2480-375.

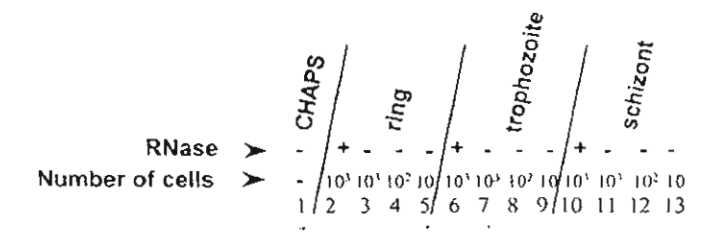
expression in the early ring stage when compared with other stages [4]. However, this observation does not correlate with either DNA synthesis or cell proliferation events in malaria parasites [5,6].

In this study, the level of telomerase activity during *P. falciparum* intraerythrocyte cycle was re-examined and the inhibitory effect of berberine against *P. falciparum* telomerase activity was also investigated. Berberine is an alkaloid found in several medicinal plants, which has been shown to inhibit DNA and RNA as well as protein synthesis in sarcoma S180 cells in vitro [7]. In addition, berberine in combination with pyrimethamine, demonstrated the best parasite clearance when compared with treatment using a combination of pyrimethamine and tetracycline or pyrimethamine and cotrimoxazole in patients with chloroquine-resistant malaria [8].

Growth of P. falciparum strain K1 [9], maintained in culture using the candle-jar technique [10], was synchronized according to the method of Lambros and Vanderberg [11]. In brief, an asynchronous culture was centrifuged at $700 \times g$ at 4 °C for 10 min. The packed erythrocytes were resuspended with 5 vol. of 5% sorbitol and left at room temperature for 10 min to allow late trophozoite- and schizont-infected erythrocytes to be lysed. The suspension was then centrifuged again. After removing the supernatant, the ring-infected erythrocytes were further cultured for approximately 24 h to obtain trophozoites and for 40 h for schizonts.

Parasites were isolated from erythrocytes by treatment with 0.15% (w/v) saponin in phosphate-buffered saline (PBS) for 10 min at 37 °C. Freed parasites were washed with RNase-free PBS. The parasite pellet containing 10⁴ cells was resuspended in 20 µl of ice-cold CHAPS solution (10 mM Tris-HCl, pH 7.5; 1 mM MgCl₂; 1 mM EGTA; 0.1 mM phenylmethylsulfonyl fluoride; 5 mM β-mercaptoethanol; 0.5% CHAPS; and 10% (v/v) glycerol). The suspension was mixed by pipetting and incubated on ice for 30 min followed by centrifuging at 12000 × g at 4 °C for 30 min. The supernatant containing telomerase was transferred to a fresh tube. Protein concentration was determined by Autokit Micro TP (Wako, Japan).

Telomerase activity of P. falciparum was determined by the telomeric repeat amplification protocol (TRAP) assay as previously described with modifications [12,13]. In brief, the assays were performed in a 25 µl of reaction mixture containing TRAP buffer (20 mM Tris-HCl, pH 8.3; 1.5 mM MgCl₂; 63 mM KCl; 0.005% Tween-20; and 1 mM EGTA); 0.1 mg/ml bovine serum albumin; 50 µM each of dATP, dGTP, dTTP and 10 µM dCTP; 50 ng of TS primer (5' AATC-CGTCGAGCAGAGTT 3'); 5 ng of NT primer (5' ATCGCTTCTCGGCCTTTT 3'); 0.005 amol of TSNT internal control template (5' AATC-CGTCGAGCAGAGTTAAAAGGCCGAGAAG-CGAT 3'); 1U Tag DNA polymerase; 2 µCi of $[\alpha^{-32}P]dCTP$ (specific activity 3000 Ci/mmol; Pharmacia-Amersham); and telomerase extract. The mixture was incubated for 30 min at 30 °C to allow telomerase to elongate the TS primer, then 50 ng of pACX primer (5' GCGCGG (CT(A/G)TACC)₃CT(A/G)AACC 3') were added and the mixture was immediately placed in a thermal cycler (Amplitron* II series 1091, USA). The polymerase chain reaction (PCR) was initiated with 1 min at 95 °C for 1 cycle to avoid primer interaction, followed by 30 cycles with a denaturation step for 1 min at 95 °C, an annealing step for 1 min at 50 °C, an extension step for 1 min at 72 °C, and 1 cycle of final extension for 6 min at 72°C. The PCR products were separated by 8% non-denaturing polyacrylamide gel-electrophoresis in Tris-borate-EDTA buffer and the gel was subsequently exposed to a phosphoimager screen at room temperature for 90 min. The TRAP products were analyzed by PhosphoImager (Molecular Dynamics, USA). The internal control product, a 36 bp band, migrated to a position below the TRAP products. To ensure that TRAP products on the gel were the results of telomerase activity, controls without extract (extract was replaced by CHAPS solution) and with RNase A pretreatment were performed for all experiments. For the RNase A control, each extract was preincubated with RNase A at a final concentration of 50 μg/ml for 20 min at 37 °C before starting the assay. Although the TS primer was designed according to human telomerase assay [12,13], it contained a few bases at the 3' end complemen-



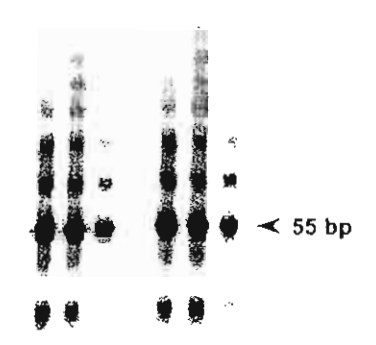


Fig. 1. Intraerythrocytic stage specificity of *P. falciparum* telomerase. *P. falciparum* was synchronized at ring stage by sorbitol, and cells were collected at different stages of parasite development and lysed by CHAPS lysis buffer. Parasite extracts were assayed for telomerase activity using the TRAP method. Lane 1 is CHAPS lysis buffer control. Lanes 2, 6 and 10 are RNase A-treated samples. The parasite stage and numbers of cells in the extracts are indicated.

tary to the putative RNA template sequence of *P. falciparum* [14]. These bases were sufficient to form a hybrid with parasite telomerase RNA template to allow polymerization to proceed.

The telomerase activities in the parasite extracts were compared using the same number of infected cells, ranging from $10-10^3$ cells per assay. Results in Fig. 1 show that telomerase activity was present in all stages of parasite development but trophozoites and schizonts contained higher activity than the ring stage. *P. falciparum* telomerase activity could still be detected in extracts from 10 trophozoites or schizonts. This is

consistent with reports that in tumor and hamster cells a higher level of telomerase activity is found during the S phase when compared with other phases of the cell cycle [15,16]. P. falciparum DNA synthesis (S phase) starts approximately 28-31 h after merozoite invasion (during early trophozoite development) and the DNA content then increases for approximately 8-10 h [6]. The findings are in agreement with the observation that telomerase activity is sustained throughout the cell cycle [4,15,16]. Although telomerase is constitutively active, this does not imply that telomerase continuously adds telomeric repeats

to telomeres, as the length of telomeres of immortalized cell lines has been found to be maintained at a constant average value [17]. Telomerase activity may be regulated by multiple mechanisms so as to add telomeric repeats to telomeres only during the appropriate period of the S phase [16].

Our results are in contrast to a previous report showing that maximum P. falciparum telomerase activity was detected during the early ring stage, with diminished activity observed at the schizont stage [4]. The difference is likely to be due to the different normalization procedures used in the two studies. We compared telomerase activity in each parasite stage based on cell numbers, whereas in the previous study telomerase activity was based on protein concentration. In our study, the protein content of 10³ parasites at various stages was 0.14 µg ring, 0.30 µg trophozoite and 0.46 µg schizont. The remarkably high telomerase activity in trophozoite and schizont stages relative to that of ring seen in the P. falciparum K1 strain used in this study may reflect the long period of adaption of this parasite isolate to continuous growth in culture [9].

To test the inhibitory effect of berberine, an alkaloid extracted and purified from Arcangelisia flava (L.) Merr., against P. falciparum telomerase activity, berberine was dissolved in dimethylsulfoxide (DMSO) and added to the telomerase assay reaction mixture. To eliminate the possible inhibitory effect of berberine on Taq polymerase, TRAP assay was conducted in two steps [18]. The first step consisted of TS primer extension in a 50 µl reaction mixture containing TRAP buffer, 50 μM of each dNTP, 100 ng of TS primer and 4 μl of telomerase extract (from 2×10^3 cells). The mixture was incubated in the thermocycler at 30 °C for 30 min in the absence or presence of different concentrations of berberine. The reaction mixture was then heated at 95 °C for 3 min to inactivate telomerase activity. The extended TS products were purified by phenol-chloroform extraction and ethanol precipitation. The precipitate was resuspended in RNase-free water and amplified by Taq polymerase. Fig. 2 shows that berberine at ≥ 150 µM caused a decrease in both the intensity and numbers of the bands. A

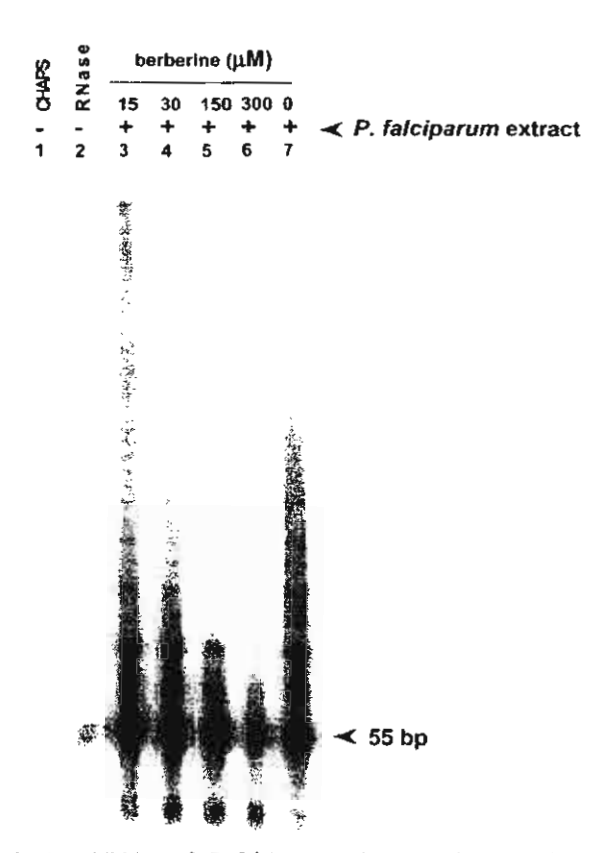


Fig. 2. Inhibition of *P. falciparum* telomerase by berberine. Berberine was added in each reaction at concentrations indicated before initiation of the process of TRAP assay. Lane 1 is CHAPS lysis buffer control. Lane 2 is *P. falciparum* extract $(2 \times 10^3 \text{ cells})$ treated with RNase A. The concentrations of berberine are indicated.

diminution of the band intensities and numbers was observed at 75 μ M berberine and *P. falci-parum* telomerase activity was completely abolished at 370 μ M berberine (data not shown). The IC₅₀ value for berberine to inhibit *P. falci-parum* growth in culture, based on incorporation of [³H]-hypoxanthine, was 2.4 μ M, suggesting that either berberine is concentrated in the parasite or that it has other effects on parasite proliferation [7].

In summary, this study confirms the presence of telomerase in *P. falciparum*, and demonstrates that the enzyme is sensitive to inhibition by the plant alkaloid, berberine. *P. falciparum* telomer-

ase offers a new potential target for future antimalarial development.

Acknowledgements

We thank Ms. P. Hirsch for her critical review of the manuscript; Ms. S. Sakdikul for technical assistance; and Ms. Daraporn Pittayakhachonwut, National Science and Technology Development Agency, Ministry of Science, Technology and Environment, Thailand for providing berberine. P.W. is a Senior Research Scholar of the Thailand Research Fund.

References

- Blackburn EH. Structure and function of telomeres. Nature 1991;350:569-73.
- [2] Meyerson M. Role of telomerase in normal and cancer cells. J Clin Oncol 2000;18:2626-34.
- [3] Bottius E, Bakhsis N, Scherf A. Plasmodium falciparum telomerase: de novo telomere addition to telomeric and nontelomeric sequences and role in chromosome healing. Mol Cell Biol 1998;18:919-25.
- [4] Aldous WK, Martin RK, Kyle DE. Stage specific detection and inhibition studies of *Plasmodium falciparum* telomerase. Mol Biochem Parasitol 1998;95:281-5.
- [5] White JH, Kilbey BJ. DNA replication in the malaria parasite. Parasitol Today 1996;12:151-5.
- [6] Arnot DE. The *Plasmodium* cell-cycle: facts and questions. Ann Trop Med Parasitol 1998;92:361-5.
- Creasey WA. Biochemical effects of berberine. Biochem Pharm 1979;28:1081-4.
- [8] Sheng WD, Jiddawi MS, Hong XQ, Abdulla SM. Treatment of chloroquine-resistant malaria using pyrimet-

- namine in combination with berberine, tetracycline or cotrimoxazole. East Afr Med J 1997:74:283-4.
- [9] Thaithong S, Beale GH. Resistance of ten Thai isolates of *Plasmodium falciparum* to chloroquine and pyrimethamine by in vitro tests. Trans R Soc Trop Med Hyg 1981;75:271-3.
- [10] Trager W, Jensen JB. Human malaria parasites in continuous culture. Science 1976;193:673-5.
- [11] Lambros C, Vanderberg JP. Synchronization of *Plas-modium falciparum* erythrocytic stages in culture. J Parasitol 1979;65:418-20.
- [12] Kim NW, Piatyszek MA, Prowse KR, Harley CB, West MD, Ho PLC, Coviello GM, Wright WE, Weinrich SL, Shay JW. Specific association of human telomerase activity with immortal cells and cancer. Science 1994;266:2011-5.
- [13] Kim NW, Wu F. Advances in quantification and characterization of telomerase activity by the telomeric repeat amplification protocol (TRAP). Nucl Acids Res 1997;25:2595-7.
- [14] Melek M, Shippen DE. Chromosome healing: spontaneous and programmed de novo telomere formation by telomerase. BioEssays 1996;18:301-8.
- [15] Zhu X, Kumar R, Mandal M, Sharma N, Sharma HW, Dhingra U, Sokoloski JA, Hsiao R, Narayanan R. Cell cycle-dependent modulation of telomerase activity in tumor cells. Proc Natl Acad Sci USA 1996;93:6091-5.
- [16] Kruk PA, Orren DK, Bohr VA. Telomerase activity is elevated in early S phase in hamster cells. Biochem Biophys Res Commun 1997;233:717-22.
- [17] Shore D. Telomerase and telomere-binding proteins: controlling the endgame. Trends Biochem Sci 1997;22:233-5.
- [18] Mutirangura A, Sriuranpong V, Termrunggraunglert W, Tresukosol D, Lertsaguansinchai P, Voravud N, Niruthisard S. Telomerase activity and human papillomavirus in malignant, premalignant and benign cervical lesions. Br J Cancer 1998;78:933-9.



Status of Red Cell Membrane Protein Phosphorylation in Thalassemia

Rutaiwan Tohtong*, Pornpimol Metheenukul and Prapon Wilairat

Department of Biochemistry, Faculty of Science, Mahidol University, Rama 6 Road, Banakok 10400, Thailand.

* Corresponding author, E-mail: scrth@mahidol.ac.th

Received 31 Oct 2001 Accepted 22 Apr 2002

ABSTRACT The steady-state levels of β -spectrin phosphorylation in HbH (α -thalassemia 1/ α -thalassemia 2), HbH/HbConstant Spring (α -thalassemia 1/HbCS, hereafter called HbH/HbCS) and nonsplenectomized β -thalassemia/HbE (hereafter called β -thal/HbE) red cells were quantitated using Western hybridization. Phosphorylation of β -spectrin serine and threonine residues from thalassemic samples was not significantly different from normal control. However, tyrosine phosphorylation was higher than normal control in HbH (p<0.01), HbH/HbCS (p<0.05) and β -thal/HbE (p<0.05) samples. Tyrosine phosphorylation of β -spectrin was observed only in the presence of vanadate, a phenomenon not hitherto reported. As tyrosine kinase activity has been linked to oxidative stress, loss of membrane lipid asymmetry and procoagulant activity of the red cell membrane, the observed increase in β -spectrin tyrosine phosphorylation of the thalassemic red cells is likely, at least in part, to account for these parameters.

KEYWORDS: Thalassemia, tyrosine phosphorylation, spectrin.

INTRODUCTION

The thalassemic red cell membranes exhibit morphological, biochemical and mechanical abnormalities due to oxidative damage induced by binding of unmatched globin chains to the cytoplasmic surface of the membrane. The rheological properties of red cells are principally controlled by the protein cytoskeleton underlying the membrane. Although both α- and β- thalassemic red cells are less deformable than normal red cells, the two cell types exhibit differences in membrane stability, namely, the maximum extent of deformation that a membrane can undergo beyond which it fragments. The \alpha-thalassemic membrane exhibits slightly increased stability whereas \(\beta \)-thalassemic membrane shows markedly decreased stability.1,2 It is believed that differences in the properties inherent to the α- and β- globin chains are the basis for the pathophysiological differences observed between αand β- thalassemic red cells.1,2

The morphology and mechanical properties of the red cell membrane are controlled by the cytoskeletal network underlying the lipid bilayer. Spectrin is the principal structural element of the red cell cytoskeleton, regulating membrane cytoskeletal functions.³ Indeed, individuals expressing a reduced level or a mutant form of spectrin, as in hereditary spherocytosis and hereditary elliptocytosis, exhibit abnormal shaped red cells with altered mechanical properties.3

Spectrin has been shown to be a substrate for a number of kinases in vitro.4 Phosphorylation sites have been mapped to 1 threonine and 3 serine residues located near the carboxy terminal of the βchain.5 Nevertheless, the role of spectrin phosphorylation in vivo is not yet fully understood. Manno et al (1995) have shown, by in vitro 32P-incorporation and mechanical assay, that the extent of spectrin phosphorylation is inversely correlated with deformability of normal ghost cells, implying a role of spectrin phosphorylation in the mechanical control of the red cell cytoskeleton.6 Based on these data, one should predict that membrane with marked reduction in deformability, such as that seen with thalassemic red cells, should exhibit a higher level of spectrin phosphorylation. In agreement with Manno's group, Erusalimsky et al (1985) reported that intact thalassemic red cells incorporate less [32P]- orthophosphate compared to normal control, suggesting a higher basal level of phosphorylation in thalassemic cells.7 However, when isolated ghost membranes, rather than intact red cells, were used in the assay, no significant difference in the extent of ³²P incorporation was observed between thalassemic and normal red cells.7

Instead of quantitating ³²P-incorporation in membrane as in previous work, in this study we

314 ScienceAsia 28 (2002)

assessed the steady-state level of β -spectrin phosphorylation in thalassemic membranes using an immunological approach. Our data showed that β -spectrin phosphorylation at tyrosine residues of HbH, HbH/HbCS and β -thal/HbE samples, was significantly greater than that of normal control.

MATERIALS AND METHODS

Patients

Normal control subjects were healthy volunteers with normal hematological profile and hemoglobin typing. Blood samples were obtained from thalassemic subjects of the Out-Patient Division, Department of Hematology, Faculty of Medicine, Siriraj Hospital, Mahidol University, Bangkok, Thailand. These patients have been identified through standard hematological criteria and had not received blood transfusion for at least 3 months prior to blood sample collection. The hematological profiles of the patients (HbH, HbH/HbCS and β-thal/HbE) are shown in Table 1.

Materials

Chemicals for red cell ghost preparation, sodium dodecyl sulfate acrylamide gel electrophoresis (SDS-PAGE) and immunoblotting were obtained from Sigma (St Louis, MO, USA). Nitrocellulose membrane was from Schleicher & Schuell (Keene, NH, USA). Monoclonal anti-phosphoserine, -phosphothreonine, and -phosphotyrosine antibodies were obtained from Sigma. Horse-radish peroxidase (HRP)-conjugated goat-anti-mouse IgG was from Dako (Glostrup, Denmark). ECL TM reagent and X-ray film were from Amersham Life Science. GS 700 imaging densitometer, SDS-PAGE and Immunoblot apparatus were from Biorad (Hercules, CA, USA).

Preparation of ghost membrane

Ghost cell preparation was adapted from the method of Dodge et al⁸, and was performed within 6 hours of blood collection. Five ml of EDTA blood

were centrifuged at 1,000 g for 10 min, after which the plasma and buffy coat were removed. The packed red cells were washed 3 times with and finally resuspended in an equal volume of isotonic buffer (140 mM NaCl, 5 mM Tris-HCl, pH 7.4), followed by lysis in 14 volumes of hypotonic buffer (7 mM NaCl, 5 mM Tris-HCl, pH 7.4, 100 mM phenylmethylsulfonyl fluoride). For the detection of tyrosine phosphorylation, packed red cells were preincubated in an equal volume of isotonic buffer containing 1 mM sodium meta-vanadate at 37 °C for 30 min, followed by washing in isotonic buffer and lysis. The lysate was then centrifuged at 10,000 g, 4°C, for 1 hour to sediment the ghost preparation, followed by 3 more washes in hypotonic buffer. The washed ghost pellets were then resuspended in sample buffer (0.125 M Tris-HCl, pH 6.8, 6% SDS, 20% glycerol, 10% β-mercaptoethanol) and boiled for 2 min prior to analysis by SDS-PAGE.

Quantitation of **B**-spectrin

Ghost membrane proteins were separated by SDS-PAGE at a constant voltage of 150 V for 1.5 hours. Gels were stained with 0.2% (w/v) Coomassie Blue R 250 in 50% (v/v) 95% ethanol and 7% (v/v) glacial acetic acid at room temperature for 30 min, and destained in 25% (v/v) 95% ethanol and 12.5% (v/v) glacial acetic. After drying, protein bands corresponding to the position of β -spectrin were quantitated using the GS 700 Imaging densitometer (Biorad) (Hercules, CA, USA).

Quantitation of phosphoserine, -threonine and -tyrosine in β -spectrin

A duplicate gel was run as described above, but instead of staining with Coomassie Blue, the gel was transferred by electroblotting onto nitrocellulose membrane at 100 V for 2 hours. The blotted membrane was incubated in blocking buffer (5% skim milk, 150 mM NaCl, 5 mM Tris-HCl, pH 8.8, 0.2% Tween 20) at 4 °C overnight, followed by a 1:2000 dilution of monoclonal antibodies against

Table 1. Hematologic data of the normal and thalassemic patients used for the determination of β-spectrin tyrosine phosphorylation.

Subjects	Hb (g/dl)	Hct (%)	MCV (fl)	MCH (pg)	MCHC (g/dl)
Normal (n=14)	12.46 ± 2.12*	37.41 ± 5.45	87.94 ± 4.51	28.36 ± 2.68	33.35 ± 1.52
HbH (n=12)	8.18 ± 2.17	29.28 ± 7.69	71.55 ± 7.44	20.03 ± 2.08	27.99 ± 1.79
HbH/HbCS (n=5)	7.82 ± 1.47	29.78 ± 4.48	79.2 ± 3.42	20.84 ± 0.76	26.2 ± 1.25
β-thal/HbE (n=12)	6.39 ± 1.91	20.42 ± 5.92	59.63 ± 4.62	18.63 ± 1.96	31.23 ± 1.74

^{*} Mean ± 5D; Hb = hemoglobin; Hct = hematocrit; MCV = mean corpuscular volume; MCH = mean corpuscular hemoglobin; MCHC = mean corpuscular hemoglobin concentration

phosphoserine, -threonine and -tyrosine in blocking buffer at room temperature for 2 hours. The membrane was washed twice with TBST buffer (150 mM NaCl, 5 mM Tris-HCl, pH 8.8, 0.2% Tween 20) for 10 min each time, before incubating with 1:1000 dilution of HRP-conjugated goat anti-mouse IgG in blocking buffer for 2 hours. After washing with TBST buffer twice, 10 min each time, the antigen-antibody complex was visualized using the ECL™ method and exposure to X-ray film. The signal corresponding to the position of \beta-spectrin was quantitated by scanning the X-ray film in a GS 700 Imaging densitometer. The amounts of phosphoserine. threonine and -tyrosine in \(\beta\)-spectrin in each sample were normalized with respect to the amounts of βspectrin.

RESULTS

The steady-state levels of β -spectrin phosphorylation at serine, threonine and tyrosine residues were determined using an immunoblot technique. Phosphorylation of β -spectrin at serine and threonine residues were not significantly different between normal control and all the thalassemic cell types examined (HbH, HbH/HbCS, β -thal/HbE). Figure 1 shows a typical set of results for normal, HbH and β -thal/HbE red cell membranes. The presence of okadaic acid did not help to increase the signal intensity, indicating that serine/threonine phosphatases were not a problem in the ghost preparation (data not shown). In addition to β -spectrin, α -spectrin reacted with the anti-phosphoserine and anti-phosphothreonine antibodies. Phosphorylation

of α-spectrin has previously been shown in low-salt extract of red cell membrane stimulated with cAMP.

Tyrosine phosphorylation of β -spectrin became evident only in the presence of vanadate, and its level was significantly higher in HbH (p<0.01), HbH/HbCS (p<0.05) and β -thal/HbE (p<0.05) compared to normal control (Table 2). Figure 2 shows the results for a set of samples from normal and β -thal/HbE red cell membranes. In addition to β -spectrin, two other membrane proteins (215 Kd and 90-100 Kd) reacted weakly with the anti-phosphotyrosine antibody; presumably these were ankyrin and band 3 respectively, based on their migration in SDS-PAGE. These two proteins have also been shown to be phosphorylated at tyrosine residues.*

DISCUSSION

The thalassemic red cell membrane offers a useful system with which to study the role of spectrin phosphorylation in regulating the mechanical

 Table 2. β-spectrin tyrosine phosphorylation in normal and thalassemic ghosts.

Subjects	Normalized values of tyrosine phosphorylation		
Normal (n=14)	0.69 ± 0.47 °		
HbH (n=12)	2.14 ± 1.74 **		
HbH/HbC\$ (n=5)	1.48 ± 0.92 ***		
β-thal/HbE (n=12)	1.35 ± 0.95 ***		

^{*} Mean + SD; ** p < 0.01 versus normal control ghost;

 $^{^{***}}$ p < 0.05 versus normal control ghost.



Fig 1. Immunoblot of ghost proteins probed with antiphosphosetine monoclonal antibody. Lane 1, normal control; lanes 2-3, HbH; Lanes 4-8, β-thal/HbE. One hundered μg of red cell membrane protein were loaded in each lane of the SDS-PAGE gel. After electrotransfer, the antibody-antigen complex was visualized by ECL method. The two bands reacted with the antibody correspond to α- and β- spectrin, as determined by SDS-PAGE and Coomassie staining of a duplicate gel.

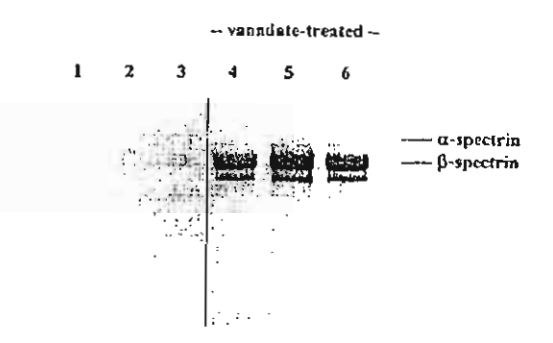


Fig 2. Immunoblot of ghost proteins probed with antiphosphotyrosine monoclonal antibody. Lanes 1 & 4, normal control; lanes 2-3 & 5-6, β-thal/HbE. One hundred µg of red cell membrane protein were loaded in each lane of the SDS-PAGE gel. After electrotransfer, the antibodyantigen reaction was visualized using ECL method. Strong immunoreaction was evident in the presence (lanes 4-6), but not in the absence (lanes 1-3), of meta-vanadate. Positions corresponding to α-spectrin and β-spectrin are indicated.

316 ScienceAsia 28 (2002)

Normal red cell membrane's deformability gradually decreases as the degree of β -spectrin phosphorylation increases, suggesting that this phenomenon is regulated by phosphorylation of β -spectrin.⁶ If that is the case, one should expect that thalassemic red cells, whose membrane deformability is markedly reduced, should exhibit a higher level of β -spectrin phosphorylation compared to that of the normal red cells. With that in mind, we have quantitated the steady-state level of β -spectrin phosphorylation in various thalassemic red cell membranes by immunoblot, as a first step towards understanding if, and how, β -spectrin phosphorylation regulates red cell membrane mechanical properties.

On 6% SDS-PAGE, α- and β- spectrin appear to be the only two major proteins that reacted with antiphosphoserine and anti-phosphothreonine antibodies. Our data show that the steady-state level of B-spectrin phosphorylation at serine and threonine residues was not significantly different between thalassemic samples and normal controls, indicating that the reduced deformability of the thalassemic red cells was not associated with \betaspectrin phosphorylation at these amino acids. Nevertheless, we cannot rule out that alterations of phosphorylation level do occur at individual sites, but the overall phosphorylation level remained unchanged, or that we failed to detect the change due to the limitation of our detection. These data are in contrast to the scenario in normal red cells as reported previously.6 Our results are, on the other hand, consistent with previous work by Erusalimsky et al, in which 32P incorporation into isolated red cell membranes of \beta-thalassemia intermedia samples was shown to be similar to that of the normal membranes, although 32P incorporation into intact thalassemic red cells was somewhat less than that of the normal cells.7

The steady-state level of β -spectrin tyrosine phosphorylation could not be detected by the immunoblot method, unless meta-vanadate was present during ghost preparation, indicating a relatively higher rate of dephosphorylation over

phosphorylation of \beta-spectrin. Although vanadate has been shown to act primarily by inhibiting protein tyrosine phosphatase9, 10, vanadium compounds have been suggested to exert multiple effects on diverse cellular processes including direct activation of tyrosine kinase11, which could probably account for the increased tyrosine phosphorylation observed. It is also possible that vanadate indirectly affects the level of β-spectrin tyrosine phosphorylation by controlling Ca2+-ATPase and hence a number of Ca2+dependent kinases which phosphorylate β-spectrin, such as casein kinase and cAMP-dependent protein kinase. Although Mg2+, Na+ and K+, but not Ca2+ ions have been shown to enhance inhibition of Ca2+-ATPase by vanadate12-14, it is not known how this reaction is modified in the thalassemic red cells, where intracellular concentrations of many ions are altered.

This is the first report of tyrosine phosphorylation of β -spectrin, although tyrosine phosphorylation of the non-erythroid homolog of spectrin, foldrin, has been reported.¹⁵ The inability of Manno et al⁶ to detect β -spectrin reactivity with anti-phosphotyrosine antibody is probably due to the lower concentration of vanadate present in their ghost preparation (10 μ M) compared to this study (1 mM).

Tyrosine phosphorylation was significantly higher than that of normal control in HbH (n=12, p<0.01), HbH/HbCS (n=5, p<0.05) and β -thal/HbE (n=12, p<0.05) samples. Tyrosine phosphorylation of membrane proteins has been implicated in regulating various functions of the red cell, including glycolysis, morphology and ion transport activity.4 16-17 Increased tyrosine kinase activity induced by oxidative stress has been observed in various cell types, including normal and pathologic red cells. In sickle-cell disease, exposing the red cells to deoxygenation resulted in increased tyrosine kinase activity, concommittant with cellular dehydration.18 Terra et al reported that the steady-state level of band 3 tyrosine phosphorylation is elevated 2-10 fold in various types of sickle cell disorder and approximately 4 fold in β-thalassemia intermedia.19 However, tyrosine phosphorylation of β-spectrin was not documented. It is possible that oxidative stress affects β-spectrin phosphorylation by modification of spectrin kinases/phosphatases, or by alterating the spatial arrangement of membrane proteins. 18-22

Reduced tyrosine kinase activity of membrane proteins is observed in Scott syndrome, a hereditary bleeding disorder characterized by a deficiency in prothrombinase activity caused by defective phospholipid scrambling activity of the blood cell membrane.²³ The decrease in membrane phospholipid scrambling results in reduction in phosphatidyl serine (PS) exposure and in prothrombinase activity on the cell surface. On the other hand, thalassemic red cells exhibit an increase in PS exposure and prothrombinase activity^{24,25}, correlating with the elevation of tyrosine kinase activity. Thus, under oxidative stress, high PS exposure and prothrombinase activity of thalassemic red cells are accompanied by increased β -spectrin tyrosine phosphorylation.

ACKNOWLEDGEMENTS

This work is supported by a grant from Faculty of Science, Mahidol University to RT and by The Thailand Research Fund Senior Researcher Award to PW.

REFERENCES

- Schrier SL (1994) Thalassemia: pathophysiology of red cell changes. Annu Rev Med 45, 211-8.
- Wilairat P, Kittikalayawong A and Chaicharoen S (1992) The thalassemic red cell membrane. Southeast Asian J Trop Med Public Health 23, 74-8.
- Knowles W, Marchesi SL and Marchesi VT (1983) Spectrin: structure, function, and abnormalities. Semin Hematol 20, 159-74.
- Cohen CM and Gascard P (1992) Regulation and posttranslational modification of erythrocyte membrane and membrane-skeletal proteins. Semin Hematol 29, 244-92.
- Harris HW and Lux SE (1980) Structural characterization of the phosphorylation sites of human erythrocyte spectrin. J Biol Chem 255, 11512-20.
- Manno S, Takakuwa Y, Nagao K and Mohandas N (1995) Modulation of erythrocyte membrane mechanical function by spectrin phosphorylation and dephosphorylation. J Biol Chem 270, 5659-65.
- Erusalimsky J, Shinar E, Rachmilewitz EA and Milner Y (1985)
 Alterations in membrane protein and phosphorylation pattern in β-thalassemic red blood cells. Ann NY Acad Sci 445, 81-91.
- Dodge JT, Mitchell C and Hanahan DJ (1963) The Preparation and chemical characteristics of hemoglobin-free ghosts of human erythrocytes. Arch Biochem Biophys 110, 119-30.
- Shechter Y (1990) Insulin-mimetic effects of vanadate possible implication for future treatment of diabetes. Diabetes 39, 1-5.
- 10. Fantus IG, Kadota S, Deragon G, Foster B and Posner BI (1989) Pervanadate [peroxide(s) of vanadate] mimics insulin action in rat adipocytes via activation of the insulin receptor tyrosine kinase. Biochemistry 28, 8864-71.
- 11. Stankiewics PJ and Tracey AS (1995) Stimulation of enzyme activity by oxovanadium complexes. In: Metal Ions in Biological Systems (Edited by Sigel H and Sigel A), vol 31, pp 249-285. Marcel Dekker, Inc, New York.
- 12. Barrabin H, Garrahan PJ and Rega AF (1980) Vanadate inhibition of the Ca²⁺ ATPase from human red cell membranes. Biochim Biophys Acta 600, 796-804.
- Bond GH and Hudgins PM (1980) Inhibition of red cell Ca ² ATPase by vanadate. Biochim Biophys Acta 600, 781-90.

14. Romero P and Rega AF (1995) Effects of magnesium plus vanadate on partial reaction of the Ca²⁺ ATPase from human red cell membranes. Biochim Biophys Acta 1235, 155-7.

- 15. Kadowaki T, Nishida E, Kasuga M, Akiyama T, Takaku F, Ishikawa M, Sakai H and Kathuria S, et al (1985) Phosphorylation of fodrin (nonerythroid spectrin) by the purified insulin receptor kinase. Biochem Biophys Res Com 127, 493-500.
- Harrison ML, Rathinavelu P, Arese P, Geahlen RL and Low PS (1991) Role of band 3 tyrosine phosphorylation in the regulation of erythrocyte glycolysis. J Biol Chem 266, 4106-11.
- Yannoukakos D, Vasseur C, Piau JP, Wajcman H and Bursaux E (1991) Phosphorylation sites in human erythrocyte band 3 protein. Biochim Biophys Acta 1061, 253-66.
- 18. Merciris P, Hardy-Dessources MD, Sauvage M and Giraud F (1988) Involvement of deoxygenation-induced increase in tyrosine kinase activity in sickle cell dehydration. Pflugers Arch 436, 315-22.
- 19. Terra HTMB, Saad MJA, Carvalho CRO, Vicentin DL, Costa FF and Saad STO (1988) Increased tyrosine phosphorylation of band 3 in hemoglobinopathies. Am J Hematol 58, 224-30.
- 20.Heffetz D, Bushkin I, Dror R and Zick Y (1990) The insulinomimetic agents H₂O₂ and vanadate stimulate protein tyrosine phosphorylation in intact cells. J Biol Chem 265, 2896-909.
- Hosey MM, Plut DA and Tao M (1978) Inhibition of protein phosphorylation and induction of protein cross-linking in erythrocyte membranes by diamide. Biochim Biophys Acta 506, 211-20
- 22. Morle L., Dorleac E., Alloisio N., Jaccoud P., Colonna P., Bachir D and Delaunay J. (1982) Kinetic alterations of the red cell membrane phosphatase in α- and β- thalassemia. Am J Hematol 13, 269-82.
- 23. Dekkers DWC, Comfurius P, Vuist WMJ, Billheimer JT, Dicker I, Weiss HJ, Zwaal RFA and Bevers EM (1998) Impaired Ca²⁺-induced tyrosine phosphorylation and defective lipid scrambling in erythrocytes from a patient with Scott Syndrome: a study using an inhibitor for Scramblase that mimics the defect in Scott Syndrome. Blood 91, 2133-8.
- 24. Yashar VB, Barenholz Y, Hy-Am E, Rachmilewitz EA and Eldor A (1993) Phosphatidylserine in the outer leaflet of red blood cells from β-thalassemia patients may explain the chronic hypercoagulable state and thrombotic episodes. Am J Hematol 44, 63-5.
- 25.Zwaal RFA and Schroit AJ (1997) Pathophysiologic implications of membrane phospholipid asymmetry in blood cells. Blood 89, 1121-32.

SHORT COMMUNICATION

Hb SIAM [α 15(A13)Gly \rightarrow Arg (α 1) (GGT \rightarrow CGT)] IS A TYPICAL α CHAIN HEMOGLOBINOPATHY WITHOUT AN α -THALASSEMIC EFFECT

Chairat Turbpaiboon, Saovaros Svasti, Phannee Sawangareetakul, Pranee Winichagoon, Chantragan Srisomsap, Noppadol Siritanaratkul, Suthat Fucharoen, Prapon Wilairat, ** and Jisnuson Svasti**.

¹Department of Biochemistry, Faculty of Science, Mahidol University, Rama 6 Road, Bangkok 10400, Thailand
 ²Thalassemia Research Center, Institute of Science and Technology for Research and Development, Mahidol University, Salaya, Nakorn Pathom 73170, Thailand
 ³Laboratory of Biochemistry, Chulabhorn Research Institute, Bangkok 10210, Thailand
 ⁴Department of Medicine, Faculty of Medicine Siriraj Hospital, Mahidol University, Bangkok 10700, Thailand

Hb Siam $[\alpha 15(A13) \text{Gly} \rightarrow \text{Arg } (\alpha 1)]$ has been described in a Chinese male from Thailand (1), and is the same mutation as Hb Ottawa that was found in a Canadian octogenarian of Polish extraction (2). The base substitution, $GGT \rightarrow CGT$ in the $\alpha 1$ -globin gene, was demonstrated for the first time in a healthy 21-year-old Thai female with Hb Siam (3). The first report (1) had a normal hematological profile, while mild anemia was observed with Hb Ottawa (2), but was believed to be due to iron and folate deficiency together with a chronic uremic state, rather than being caused by the variant. The second case of Hb Siam was also healthy, but had a compound heterozygosity for α-thalassemia-1 (α-thal-1), resulting in moderate microcytosis and hypochromia (3), with a hematological profile typical of an α-thal-1 heterozygote, rather than Hb H disease with one functional α-globin gene. The abnormal hemoglobin (Hb) level was 15% in

^{*}Corresponding author. Fax: +662-248-0375; E-mail: scpwl@mahidol.ac.th

the first case of Hb Siam and 20–25% in the case with Hb Ottawa. However, a higher level of 33% was found in the second case of Hb Siam, since only two α -globin genes remained (4).

Thus, information from these three cases suggest that the Hb Siam and Hb Ottawa mutations have no α -thalassemic effect per se. This paper reports another case of a healthy Thai female with the following steady state hematological profile: Hb 10.3 g/dL; MCV 64 fL; MCH 19.3 pg; MCHC 32.4 g/dL; RDW 16.3%. Hb typing by automatic high performance liquid chromatography (HPLC) (VARIANTTM; Bio-Rad Laboratories, Hercules, CA, USA) revealed two major peaks: Hb A at a retention time of 2.41 minutes and an unknown abnormal Hb present at a level of 16.6% at 4.62 minutes. Hb A2 at 3.72 minutes was 5.5%, which is higher than the normal level. Her father's steady state hematological profile was as follows: Hb 13.7 g/dL; MCV 90 fL; MCH 30.5 pg; MCHC 33.9 g/dL; RDW 16.0%, but her sister's hematological profile was Hb 11.3 g/dL; MCV 75.5 fL; MCH 24.5 pg; MCHC 32.5 g/dL; RDW 16.5%. Hb typing of her father and sister also showed two major peaks at the same positions and levels as Hb A and the unknown Hb as in the proband, except that the Hb A2 level was normal. The increased Hb A_2 in the proband suggests a β -thal heterozygote, and since Hb A is still present, the abnormal Hb inherited from the father is likely to occur on the α -globin chain.

The abnormal (α^{X}) and normal (α^{A}) chains were isolated (3), and then digested with trypsin. Peptide maps were compared by HPLC (510; Waters, Milford, MA, USA) (3). The abnormal Hb showed the tetrapeptide Ala-Ala-Trp-Arg, indicating a Gly → Arg replacement at residue 15, which we have previously described as Hb Siam (3). DNA was isolated from peripheral leukocytes by phenol-chloroform extraction (5). Segments of the α1- and α2-globin genes were selectively amplified on a DNA Thermal Cycler (Perkin Elmer Corporation, Foster City, CA, USA) using the following primers: 5'-GATGCACCCACTGG-CACTCCT-3' (C10) and 5'-CCATTGTTGGCACATTCCGG-3' (C3) for the α2-globin gene, and primers C10 and 5'-CCATGCTGGCACGTTTCTGAG-3' (C2) for the α1-globin gene. Automated DNA sequence analyses of the selectively amplified α1- and α2-globin polymerase chain reaction (PCR) products were performed using 5'-CGCTCGCGGCCCGGCACT-3' (ASL) as sequencing primer. The results showed no mutation in the α 2-globin gene, but the α 1-globin gene showed both C and G as the first base of codon 15 (Fig. 1). This indicates the replacement of GGT (Gly) by CGT (Arg) in the α 1-globin gene, consistent with the amino acid interchange observed in Hb Siam $[\alpha 15(A13)Gly \rightarrow Arg]$. Since both C and G were found at the first base of codon 15 in the α1-globin gene, it may be inferred that both α1 genes were still intact (no deletion). Certain silent mutations in the heterozygous state were found in the α2-globin sequences, suggesting that both α2-globin genes were also intact (data not shown). Thus, there was no deletion in either of the α -globin genes, which is the most common etiology of α-thal in Thailand. The proband's lower MCV and higher Hb A2 levels suggested a β -thal anomaly, that was confirmed as being due to the β^0 -thal

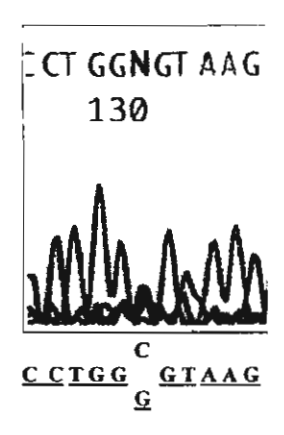


Figure 1. Automated DNA sequence analysis of the selectively amplified α1 gene showing the sense strand in the vicinity of codon 15 of the proband with Hb Siam.

mutation at codon 17 [AAG (Lys) \rightarrow TAG (stop)] in the heterozygous state. Therefore, the proband was a double heterozygote for the $\alpha 1^{\text{Siam}}$ and (β^0) codon 17 (A \rightarrow T) (6) mutations, the first such case described, while her father and sister were ordinary heterozygotes for $\alpha 1^{\text{Siam}}$.

The Hb Siam content of this family averaged 17%, similar to the 15% reported in the first report of Hb Siam (1), and about half of the 33% found in the second Hb Siam (3) case, who had only two functional α -globin genes instead of four. These values are less than expected from the number of functional genes alone, since one α^{Siam} gene from a total of four or two functional α genes is expected to lead to a Hb Siam content of 25 or 50%, respectively. The decreased level of Hb Siam observed in the Thai probands may, at least in part, be explained by the fact that the α^{Siam} mutation reported here and by Yodsowan et al. (3) lies on the α 1 gene, that has lower levels of mRNA than the α 2 gene (4,5). Using the ratios of α 1: α 2-mRNA, variously estimated as 2:3 (4) and 1:2.8 (7), the %Hb Siam expressed from α 1-mRNA would be predicted to be 20 and 13% of total Hb, respectively, assuming one α 1 siam gene out of four α genes to be present.

However, other explanations cannot be entirely ruled out, such as the mild instability of Hb Siam. On the other hand, the level of Hb Siam in association with β -thal in the proband is similar to the level of Hb Siam in the father and sister who do not have β -thal. So with $\alpha^{\rm Siam}$, there appears to be no decrease in the combination of α and β chains, even under conditions of decreased β chain expression. This is consistent with increased positive charge of the α chain due to the Gly \rightarrow Arg mutation, since it has been proposed that assembly of the $\alpha\beta$ dimer involves electrostatic interaction between the positively charged α chain and negatively charged β chain (8). Interestingly, the Hb Ottawa level observed was higher at 20–25% (2) and closer to the expected 25%, if the genes are expressed

equally, but there is no information on whether the mutation observed in Hb Ottawa was in the $\alpha 1$ or the $\alpha 2$ gene, and indeed, some α chain mutations have been found in both the $\alpha 1$ and the $\alpha 2$ genes (9).

It is also noteworthy that the proband with the double heterozygosity for $\alpha 1^{Siam}$ and (β^0) codon 17 $(A \rightarrow T)$ (6) had a hematological profile typical of heterozygous β -thal alone, where the MCV value was not affected by combination with the $\alpha 1^{Siam}$ allele, unlike the lower MCV levels found in a typical double heterozygote for α - and β -thal (10). Similarly, the hematological profile of the father was normal, including Hb and MCV levels, while the lower MCV and Hb levels in the sister may be attributed to iron deficiency anemia. This data suggests that the $\alpha 1^{Siam}$ mutation does not have an α -thalassemic effect.

ACKNOWLEDGMENTS

This work was supported by a grant from the National Center for Genetic Engineering and Biotechnology, Bangkok, Thailand (BT-38-06-HIM-14-17) to Pranee Winichagoon, and a grant from the Chulabhorn Research Institute, Bangkok, Thailand, to Jisnuson Svasti. Jisnuson Svasti and Prapon Wilairat are Senior Research Scholars of the Thailand Research Fund, Bangkok, Thailand.

REFERENCES

- 1. Pootrakul, S.; Srichayanont, S.; Wasi, P.; Suanpan, S. Hemoglobin Siam ($\alpha_2^{15\text{Arg}}\beta_2$): a new α -chain variant. Hum. Genet. 1974, 23, 199-204.
- 2. Vella, F.; Casey, R.; Lehmann, H.; Labossiere, A.; Jones, T.G. Hemoglobin Ottawa: $\alpha_2 15(A13)$ Gly \rightarrow Arg β_2 . Biochim. Biophys. Acta 1974, 336, 25–29.
- Yodsowan, B.; Svasti, J.; Srisomsap, C.; Winichagoon, P.; Fuchareon, S. Hb Siam [α15(A13)Gly → Arg] is a GGT → CGT mutation in the α1-globin gene. Hemoglobin 2000, 24 (1), 71-75.
- Orkin, S.H.; Goff, S.C. The duplicated human α-globin genes: their selection expression as measured by RNA analysis. Cell 1981, 24, 345-351.
- Sambrook, J.; Fritsch, E.F.; Maniatis, T. Molecular Cloning: A Laboratory Manual (2nd edition); Cold Spring Harbor Laboratory Press: Cold Spring Harbor, N.Y., USA, 1989.
- Chang, J.C.; Kan, Y.W. β⁰ Thalassemia, a nonsense mutation in man. Proc. Natl. Acad. Sci. USA 1979, 76, 2886–2889.
- Liebhaber, S.A.; Cash, F.E.; Main, D.M. Compensatory increase in α1-globin gene expression in individuals heterozygous for the α-thalassemia 2 gene deletion. J. Clin. Invest. 1985, 76, 1057-1064.
- 8. Mrabet, N.; McDonald, M.J.; Turci, S.; Sarkar, R.; Szabo, A.; Bunn, H.F. Electrostatic interaction governs the dimer assembly of human hemoglobin. J. Biol. Chem. 1986, 261, 5222-5228.

- 9. Old, J.M.; Higgs, D.R. The thalassemias; gene analysis. Methods Hematol. 1983, 6, 74–102.
- 10. Fucharoen, S.; Winichagoon, P.; Thonglairuam, V. β-Thalassemia associated with α-thalassemia in Thailand. Hemoglobin 1988, 12 (5&6), 581-592.

Received June 19, 2001 Accepted August 21, 2001



Biochemical Pharmacology 64 (2002) 91-98

Biochemical Pharmacology

Membrane heme as a host factor in reducing effectiveness of dihydroartemisinin

Phantip Vattanaviboon^{a,*}, Noppadol Siritanaratkul^b, Jidapa Ketpirune^b, Prapon Wilairat^c, Yongyuth Yuthavong^d

^aFaculty of Medical Technology, Department of Clinical Microscopy, Mahidol University, Siriraj Hospital, Bangkok 10700, Thailand ^bDivision of Hematology, Department of Medicine, Faculty of Medicine, Siriraj Hospital, Bangkok 10400, Thailand ^cFaculty of Science, Department of Biochemistry, Mahidol University, Bangkok 10400, Thailand ^dNational Science and Technology Development Agency, Bangkok 10700, Thailand

Received 28 November 2001; accepted 17 April 2002

Abstract

Plasmodium falciparum infecting α -thalassemic erythrocytes are resistant to artemisinin and its derivatives. Binding of the drug to hanglobin H resulting in drug inactivation was previously demonstrated. We now show that an additional host factor, membrane heme, anihoantly accounted for decreased antimalarial activity of artemisinin. The antimalarial activity of dihydroartemisinin in the presence fromal and thalassemic erythrocyte membranes showed a correlation with the heme content of the membrane ($r^2 = 0.466$, P < 0.01). The correlation was more clearly seen when the drug effectiveness was correlated with the heme content of α -thalassemic membrane ($r^2 = 0.636$, P < 0.01). However, the drug effectiveness showed no correlation to ferrozine-reactive (free or non-heme) iron content ($r^2 = 0.0001$, $r^2 = 0.0001$). A-Thalassemic erythrocytes contained higher amounts of membrane heme (11.04 \pm 8.96 nmol/mg membrane protein) than those from normal and $r^2 = 0.001$. Loss of drug effectiveness was also correlated with increment of heme content in membrane prepared from normal erythrocytes treated with phenylhydrazine. It is concluded that heme in both normal and thalassemic erythrocyte membranes is an important factor in drug inactivation. © 2002 Elsevier Science Inc. All rights reserved.

Keywords: Artemisinin; Heme; Thalassemia; Malaria

1. Introduction

Artemisinin (Fig. 1) and its derivatives form a promising class of antimalarial drugs, which are now commonly used in the treatment of falciparum malaria [1,2]. Dihydroartemisinin (DHART, Fig. 1) is a derivative of artemisinin with the C-10 lactone group replaced by hemiacetal. It is more effective antimalaria than artemisinin, and is the active methodite of a number of artemisinin derivatives. They are widely used in Thailand, Myanmar, Vietnam and China, where multidrug resistant parasites are common [3]. Up to the present, there has been no report of resistance to artemisinin and its derivatives in the treatment of falci-

parum malaria despite widespread clinical application [4,5]. Our previous studies have demonstrated the role of α-thalassemic erythrocytes, both of HbH and HbH/ HbCS types, in reducing artemisinin effectiveness [6-8]. DHART, which apparently acts in a similar manner to artemisinin [4,5], also showed the same reduction in effectiveness with these erythrocytes [8]. It was found that the reduction in drug effectiveness is partly due to higher drug accumulation capacities of uninfected α-thalassemic erythrocytes than genetically normal cells and to drug inactivation by \alpha-thalassemic erythrocytes. Greater drug binding affinity of hemoglobin H in the α-thalassemic erythrocytes than hemoglobin A partly accounts for the high drug accumulation capacities. Hemolysates, purified hemoglobin H and erythrocyte membranes have also been demonstrated to account for preferential drug inactivation [7]. Intact cells and the membrane compartment of \(\beta - \) thalassemia/HbE erythrocytes also had the capacity to inactivate the drug, albeit to a much lesser extent [7].

Corresponding author. Tel.: +662-419-7169; fax: +662-412-4110.

E-mail address: mtpvt@mahidol.ac.th (P. Vattanaviboon).

Abbeviations: HbH, α-thalassemia 1/α-thalassemia 2; HbH/HbCS, α-thalassemia 1/hemoglobin constant spring; α-thal, both HbH and HbH/HbCS: β-thal/E, β-thalassemia/HbE; DHART, dihydroartemisinin; 1C₅₀.

809 Inhibitory concentration; ρ², correlation coefficient; P, P-value.

Fg. I. Artemisinin (A) and its lactol derivatives (B) including dihydroartemisinin (R=H), artemether (R=CH₃), arteether (R=CH₂CH₃) and artesunate [R=CO(CH₂)₂CO₂Na].

Since the action of artemisinin is likely initiated by heme or molecular iron [9] and both heme and non-heme iron contents were reported to be present in higher amounts in thalassemic erythrocyte membranes than normal membranes [10,11], they can be significant factors interfering with artemisinin effectiveness. Premature activation of the drug outside the malaria parasite by erythrocyte components would lead to reduced effectiveness. Such interference, together with other contributing causes, may further lead to the development of true artemisinin resistance due to exposure of the parasite to sublethal drug concentrations. We present here the evidence that heme but not nonheme iron is the major factor in erythrocyte membrane causing reduction in effectiveness of DHART in both αthalassemic and normal erythrocytes in which the heme content was artificially increased.

2. Materials and methods

2.1. Materials

Iron-free glassware was prepared by soaking in 50% hydrochloric acid overnight and then rinsing with deionized water [12]. Reagents used in sample preparations and mon study were prepared iron-free by using chelating resin (Chelex 100). Plasticware was purchased as iron-free grade (Axygen).

2.2. Samples

Heparinized blood samples were collected from 22 α-halassemic patients (10 HbH and 12 HbH/HbCS patients, males, 14 females) and 11 β-thalassemia/HbE patients (7 males, 4 females) from Division of Hematology, Department of Medicine, Faculty of Medicine, Siriraj Hospital, Mahidol University, where hematologic parameters and hemoglobin typing were obtained. Normal blood samples were also collected voluntarily from nine healthy individuals (four males, five females) with normal hemoglobin

typing. All subjects were non-splenectomized, ages during 20-50 years and had not been transfused for at least 3 months before the study. No subjects had previous history of malarial infection.

The samples were processed within 2 hr. Whole blood was centrifuged at 800 g, at 4° for 15 min, after which plasma and buffy coat were removed. To study drug inactivation by intact erythrocyte, the packed erythrocytes were washed for three times with serum-free culture medium (RPMI 1640 medium supplemented with 25 mM HEPES, pH 7.4, 0.2% NaHCO₃, 40 μg/mL of gentamicin) and resuspended to give 50% cell suspension in serum-free culture medium. For membrane studies, the erythrocytes were washed three times with ice-cold iron-free phosphate buffer saline (PBS, pH 7.4). Ghost membrane preparation was performed as described by Kuross and Hebbel [13]. Erythrocytes were lysed with ice-cold lysis buffer (5 mM phosphate buffer, 0.5 mM EDTA, pH 8.0, iron-free). Membrane was separated by centrifugation (10,000 g, at 4° for 15 min). The ghosts were extensively washed five times with ice-cold lysis buffer with multiple passages of the ghost pellet through 23 Gauge needle between washes and then twice with ice-cold washing buffer (5 mM phosphate buffer, pH 7.4, iron-free). The membrane was resuspended in 1 mL ice-cold washing buffer and kept in <-20° until further experiments within 1 month.

2.3. Studies of dihydroartemisinin (DHART) inactivation by intact erythrocyte and membrane

To study the effect of intact erythrocyte on antimalarial activity of DHART, 70 μ L of packed erythrocytes were incubated at 37° for 2 hr with 630 μ L of radioactive [14 C]-DHART (a kind gift from Kenneth H. Davis, Jr., Chemistry and Life Sciences Division, Research Triangle Institute, NC, USA, specific activity 12.1 Ci/mol) in serum-free culture medium at final concentration of 1 μ M [8]. For study of membrane effect, 200 μ L of 1 mg/mL membrane protein (200 μ g, equivalent to membranes prepared from 70 μ L packed erythrocytes) were incubated with 800 μ L of

radioactive drug (1 μ M final concentration) in the same ndition as intact cells. At the end of the incubation, intact Is or membranes were pelleted by centrifugation at .000 g at 4° for 3 min. Amount of drug remaining in supernatant was determined from its radioactivity. An quot of 500 μ L supernatant was bleached with 500 μ L of % H_2O_2 at 60° for 12 hr; 4 mL of Triton-based liquid ntillation fluid were added. The radioactivity was meared in a β -counter (LS1801, Beckman Instrument Inc.) d used for calculation of drug concentration in the pernatant. This drug concentration in the supernatant is then used as the starting drug concentration in the dy of drug effectiveness which was determined from its timalarial activity.

4. Antimalarial activity assay

Antimalarial activity of the drug in the supernatant was sayed by using the [3H]-hypoxanthine incorporation ethod of Desjardins et al. [14]. An aliquot (25 µL) of propriate dilution of the supernatant (ranging from 0.1 to 0 nM DHART) was pipetted into 96 flat-bottom well icrotitration plate. Parasitized erythrocyte suspensions intaining 1.5% hematocrit with 1-2% parasitemia at the rly ring stage were added (200 µL each well). After 24-hr cubation in a candle jar at 37°, 25 µL of [3H]-hypoxthine (0.5 µCi, specific activity 20-30 Ci/mmol, Ameriam) were added into each well and the plate was cubated for another 18 hr under the same condition. arasitic DNA was harvested onto glass filter paper (Whatan) by using cell harvester (Nunc). Each paper disk was ashed with distilled water, dried and placed in tolueneased scintillation fluid for counting in β-counter. The 50% hibitory concentration (1C50) value was evaluated from e sigmoid graph of percent [3H]-hypoxanthine incorration vs. log of drug concentration. The drug effectivess index was calculated from the ratio of 1050 of control rug without cell or membrane)/1C50 of sample.

5. Measurement of membrane iron

Each membrane sample was diluted with 5 mM phoshate buffer (pH 7.4, iron-free) to an equivalent of 1 mg/ IL of protein. An aliquot of 100 μL of erythrocyte memrane (100 μg) was used for each iron assay. Free or non-eme iron in membrane samples was determined by its activity with an iron chelator, ferrozine (Sigma) by the ethod of Kuross and Hebbel [13]. Free iron can rapidly act (within 2 min) with ferrozine in the presence of adium dodecylsulfate (SDS) and reducing agents (ascoric acid and sodium metabisulfite). Absorbance of the action was measured at 562 nm. Amounts of free iron recalculated and expressed as nmol-free iron/mg memane protein. Total heme (i.e. free heme, hemoglobin, emichrome) in membranes was measured by the absortance at 398 nm after dissolving membrane samples in

formic acid [13]. Amounts of heme iron were calculated using a hemoglobin standard (Biosystem) and expressed as nmol heme iron/mg membrane protein.

The protein contents of erythrocyte membrane samples were determined by the method of Lowry *et al.* [15] with bovine serum albumin as standard (Sigma).

2.6. DHART inactivation and membrane iron content in phenylhydrazine-treated normal erythrocyte

To study the possible mechanism of drug inactivation in α -thalassemic erythrocytes, 20% cell suspension of normal erythrocytes in serum-free culture medium was oxidized by adding 1, 10 or 100 μ M phenylhydrazine hydrochloride (BDH) in PBS. The mixtures were incubated at 37° for 1 hr. Control cells were treated under the same condition without phenylhydrazine hydrochloride. After incubation, the erythrocytes were washed thrice with serum-free culture medium and resuspended for drug inactivation assay and iron assay as described above.

2.7. DHART accumulation and distribution in oxidized erythrocytes

To study the effect of oxidative stress on drug accumulation and distribution in the cell, normal and thalassemic erythrocytes were treated with 0.1 and 1.0 mM phenylhydrazine hydrochloride and washed by the same procedure as described above. Two sets of duplicate aliquots (70 µL each) of packed-treated erythrocytes were incubated with [14C]-DHART (at final concentration of 1 µM) by the same procedure as the study of drug inactivation by intact erythrocyte. After incubation, the erythrocytes were pelleted and washed thrice with 1.0 mL serum-free culture medium. One set of erythrocytes was lysed with 2% SDS (500 µL each) and bleached with 500 µL of 15% H2O2 at 60° for 12 hr. The radioactivity of accumulated drug was measured by a \beta-counter after adding 4 mL of Tritonbased liquid scintillation fluid. For drug distribution measurement, another set of erythrocytes was lysed with 10 vol. of lysis buffer. An aliquot of 500 µL lysate was incubated with an equal volume of 2% SDS prior to bleaching and radioactivity counting as described above. The membranes were washed five times with 1.0 mL of washing buffer and the above process was followed for radioactivity determination. Amounts of the drug accumulated and distributed in the erythrocytes were calculated as pmol/106 cells.

2.8. Statistical analysis

The statistical differences of the data were determined by using Mann-Whitney *U*-test for independent data and Sign-Rank test for dependent data. Correlation of parameters studied was determined from linear regression analysis.

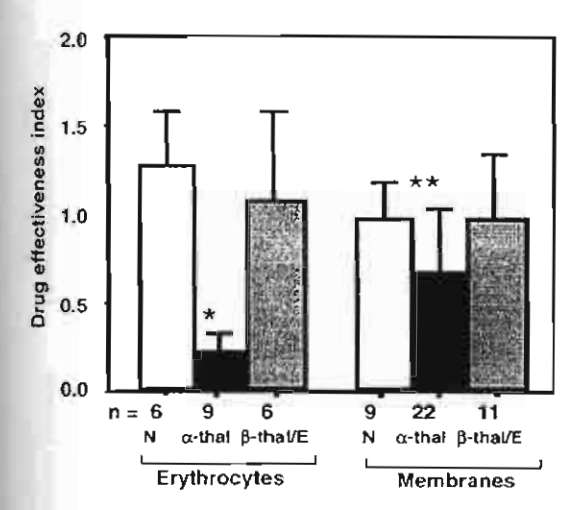


Fig. 2. Antimalarial effectiveness of DHART in the supernatant after acubating the drug (1 μ M) with intact cells or membrane compartments of somal or thalassemic crythrocytes at 37° for 2 hr. The drug activity was measured by 1 HJ-hypoxanthine incorporation assay. The drug effectiveness index was calculated from the ratio of 1_{50} of control (drug without cell or membrane)/ 1_{50} of sample. Columns represent mean \pm SD. * P < 0.01, ** P < 0.02 when comparing α -thalassemia with the other cells or embranes; N represents normal samples in the study. For α -thalassemia, there were 4 HbH and 5 HbH/HbCS subtypes for the group of N = 9 and 10 HbH and 12 HbH/HbCS subtypes for the group of N = 22.

3. Results

3.1. Dihydroartemisinin inactivation by intact erythrocytes ~

It was earlier shown [7.8] that, similarly to the reduction of effectiveness of artemisinin by α -thalassemic erythrotytes, the effectiveness of DHART is also reduced. We show here further (Fig. 2) that a part of the reduction in effectiveness was due to preferential inactivation of the drug since pre-incubation with these erythrocytes resulted in reduced effectiveness of the free drug in the supernatant (P < 0.01). As shown in Fig. 2, the drug effectiveness index of DHART after incubation with both types of α -thalassemic erythrocytes was five times lower than that after incubation with normal or β -thalassemia/HbE erythrocytes.

31. Dihydroartemisinin inactivation by \alpha-thalassemic envirocyte membrane

Our previous report demonstrated that both α - and β -thatassemic erythrocyte hemolysates could inactivate artemisinin to greater extent than that of the normal hemolysate [7]. We now show that the membrane component of α -thatassemic erythrocytes was also involved in artemisinin fractivation. Significant reduction of DHART activity was demonstrated after incubating the drug with 200 μ g membrane protein (Fig. 2, P < 0.02). Intact α -thatassemic crythrocytes could reduce the effectiveness of DHART by more than 80%, while the membrane fraction accounted for about 35% of the reduction.

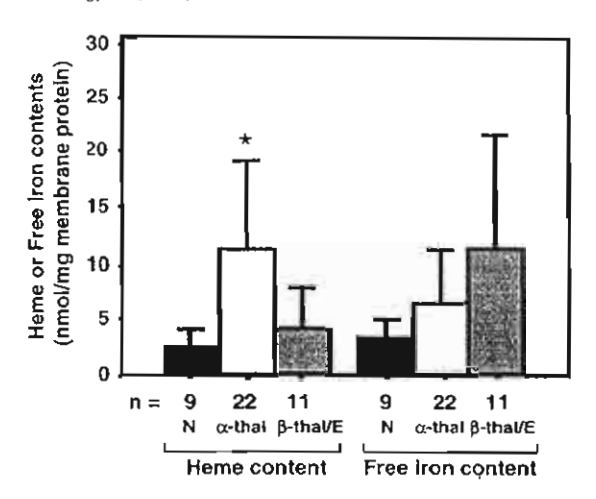


Fig. 3. Total heme and free iron contents in normal and thalassemic membranes. Free iron in membrane samples was determined from its reactivity with an iron chelator, ferrozine, and measuring the absorbance at 562 nm. Total heme was measured by the absorbance at 398 nm after dissolving membrane samples in formic acid. Columns represent mean \pm SD. "P < 0.01 when comparing α -thalassemic membrane heme content with the other cell types; N represents normal samples in the study. The α -thalassemia group comprised 10 HbH and 12 HbH/HbCS subtypes.

3.3. Ferrozine-reactive iron and heme iron content in erythrocyte membranes

Membrane iron components, heme or non-heme, which are known to be present in higher amount in α-thalassemic erythrocytes than normal erythrocytes [10,11], may be significant factors in reducing drug effectiveness. In order to investigate this possibility, both free (non-heme) ironand heme iron-bound membrane were determined. Fig. 3 shows the amounts of both forms of membrane iron in the various cell types. Although there was a wide variation in the free and heme-bound iron contents of the membranes (Fig. 3), it was found that α-thalassemic erythrocyte membrane contained significantly higher heme iron content (11.04 \pm 8.96 nmol/mg membrane protein, P < 0.01) than membranes from normal (2.68 ± 1.28 nmol/mg membrane protein) or B-thalassemia/HbE erythrocytes (3.98 ± 3.98 nmol/mg membrane protein). Decrease in drug effectiveness by membrane was correlated to membrane heme content ($r^2 = 0.460$, P < 0.01, Fig. 4A) whereas there was no correlation with free iron content $(r^2 = 0.0001, P > 0.05, \text{Fig. 4B})$. The correlation between reduction in drug effectiveness index and membrane heme content was more clearly evident for a-thalassemic erythrocytes ($r^2 = 0.636$, P < 0.01, Fig. 4C). This indicated that membrane heme was an important factor accounting for drug inactivation by α-thalassemic erythrocytes.

3.4. Role of oxidative stress on membrane heme content, hemoglobin denaturation and DHART ineffectiveness

Under oxidative stress, hemoglobin H may be oxidized, and this oxidized form is associated with cellular

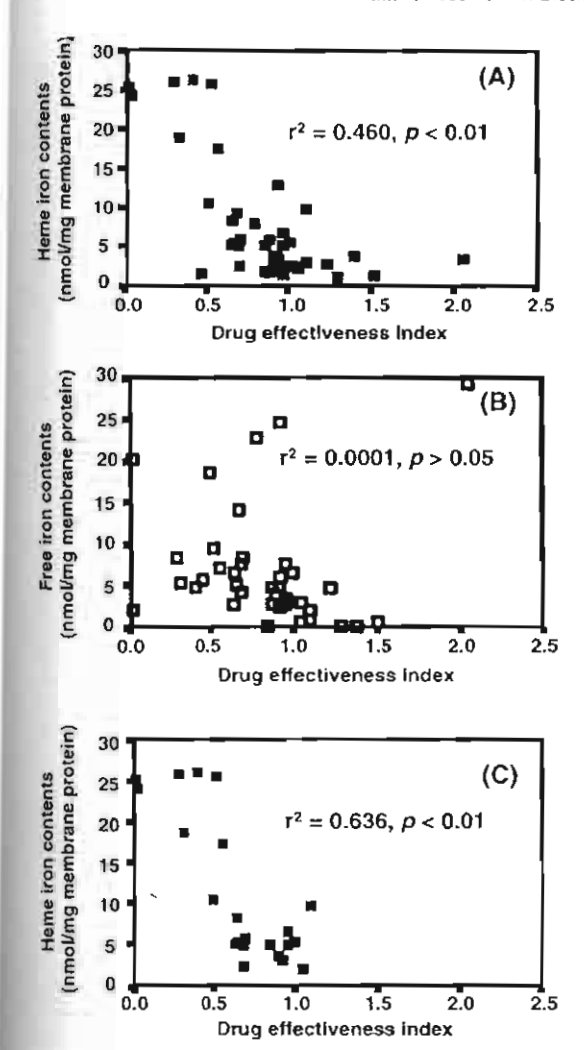


Fig. 4. Correlation of antimalarial effectiveness with membrane heme or iron contents. (A) Correlation of antimalarial effectiveness with membrane heme contents of all samples; (B) lack of correlation of antimalarial effectiveness with membrane-free iron contents of all samples; (C) increased correlation of antimalarial effectiveness with membrane heme contents of α -thalassemic membrane.

membrane [11.16]. In order to investigate the role of oxidative stress on membrane heme and drug ineffectiveness, normal erythrocytes were oxidized with various concentrations of phenylhydrazine. Upon oxidation, hemoglobin is oxidized and denatured to monomeric globin which can associate with cell membrane and causes membrane pathology [17]. After incubating DHART with oxidized genetically normal erythrocytes, the drug effectiveness index decreased in a dose-dependent manner and was significantly reduced when the cells were treated with $\geq 10~\mu M$ phenylhydrazine (P < 0.015, Fig. 5). Fold increment of the membrane heme and free iron contents (membrane heme or free iron content of oxidized cells/that of control cells) also directly depended on phenylhydrazine concentration. However,

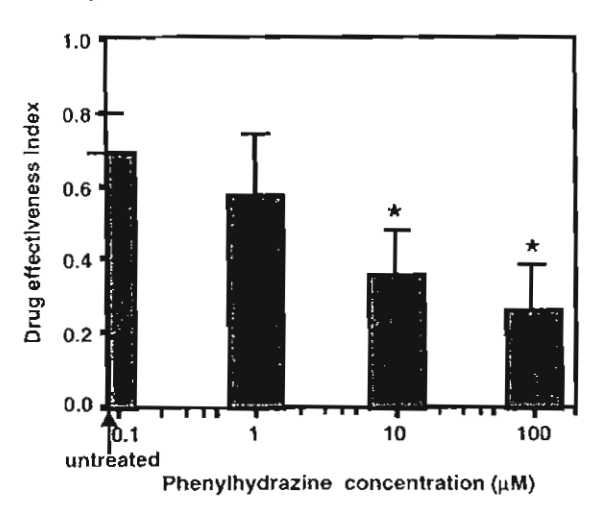


Fig. 5. Antimalarial effectiveness of DHART (1 μ M) after incubating with phenylhydrazine-treated and untreated normal erythrocytes (N = 8). Columns represent mean \pm SD. *P < 0.015 when comparing treated cells with untreated cells.

there was a higher increase of heme content compared to that of free iron (Fig. 6).

3.5. Role of oxidative stress on drug accumulation and distribution in erythrocytes

α-Thalassemic erythrocytes accumulate artemisinin or its derivatives to a greater extent than normal and β-thalassemia/HbE erythrocytes [7]. After treatment of normal and thalassemic erythrocytes with various concentrations of phenylhydrazine, all treated erythrocytes took up more labeled DHART in a dose-dependent manner than control untreated cells (Fig. 7A). DHART accumulation in intact cells showed significant differences between cells

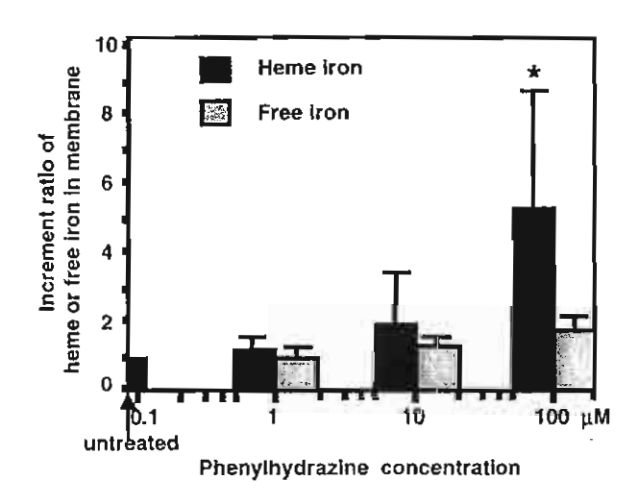


Fig. 6. Increment ratio of heme or free iron contents in membranes of phenylhydrazine-treated normal erythrocytes comparing to untreated cells (N=8). Columns represent mean \pm SD of increment ratio. *P<0.015 when comparing treated cells with untreated cells.